Distributed Optical Fiber Vibration Sensor Based on Rayleigh Backscattering

by

Zengguang Qin

Thesis submitted to the
Faculty of Graduate and Postdoctoral Studies
In partial fulfillment of the requirements for the Degree of

Doctor of Philosophy

in

Physics

Ottawa-Carleton Institute for Physics
University of Ottawa

To my family

Abstract

This thesis includes studies of developing distributed optical fiber vibration sensor based on Rayleigh backscattering with broad frequency response range and high spatial resolution.

Distributed vibration sensor based on all-polarization-maintaining configurations of the phase-sensitive optical time domain reflectometry (OTDR) is developed to achieve high frequency response and spatial resolution. Signal fading and noise induced by polarization change can be mitigated via polarization-maintaining components. Pencil-break event is tested as a vibration source and the layout of the sensing fiber part is designed for real applications. The spatial resolution is 1m and the maximum distance between sensing fiber and vibration event is 18cm.

Wavelet denoising method is introduced to improve the performance of the distributed vibration sensor based on phase-sensitive OTDR in standard single-mode fiber. Noise can be reduced more effectively by thresholding the wavelet coefficient. Sub-meter spatial resolution is obtained with a detectable frequency up to 8 kHz.

A new distributed vibration sensor based on time-division multiplexing (TDM) scheme is also studied. A special probe waveform including a narrow pules and a quasi-continuous wave can combine the conventional phase-sensitive OTDR system and polarization diversity scheme together in one single-mode fiber without crosstalk. Position and frequency of the vibration can be determined by these two detection systems consecutively in different time slots. Vibration event up to 0.6 MHz is detected with 1m spatial resolution along a 680m single-mode sensing fiber.

Continuous wavelet transform (CWT) is investigated to study the non-stationary vibration events measured by our phase OTDR system. The CWT approach can access both frequency and time information of the vibration event simultaneously. Distributed vibration measurements of 500Hz and 500Hz to 1 kHz sweep events over 20 cm fiber length are demonstrated using a single-mode fiber.

Optical frequency-domain reflectometry (OFDR) for vibration sensing is proposed for the first time. The local Rayleigh backscatter spectrum shift in time sequence could be

used to determine dynamic strain information at a specific position of the vibrated state with respect to that of the non-vibrated state. Measurable frequency range of 0-32 Hz with the spatial resolution of 10 cm is demonstrated along a 17 m fiber.

Acknowledgments

I have been extremely lucky to learn from a number of advisors and colleagues during my Ph.D. study.

First and foremost, I would like to thank my supervisor, Prof. Xiaoyi Bao, for her guidance and support throughout my Ph.D. study over the past four years. I am deeply impressed by Prof. Bao's profound knowledge, invaluable experience as well as kindness. She gave the greatest encouragement and support to me when I started my research in fiber optics group. I feel that she is always available to inspire me, give suggestions and share ideas with me. Her diligence and passion in research help me cultivate my own scientific research ability and scientific spirit which are extremely important in the future. I also would express my great gratitude to Prof. Liang Chen for his instructive and insightful suggestions during my research process. I find enormous benefits from his broad perspective and rigorous thinking.

I would like to appreciate Dr. Tao Zhu, Dr. Da-Peng Zhou, and Dr. Wenhai Li for their help. It is a memorable experience to work together with them on several exciting research projects.

I would also like to thank Dr. Yongkang Dong, Dr. Meng Pang and Dr. Ping Lu for their thoughtful discussions and valuable suggestions. Their sense to research ideas and insightful views inspire me on my own research topic.

Special thanks to Prof. Xingyu Zhang for his guidance and help during my graduate studies at Shandong University. I would like to acknowledge funding support by the China Scholar Council over the past four years.

Finally, I would like to give my deepest gratitude to my parents and my wife for their understanding, encouragement and support for all of these years! I dedicate this dissertation to them.

Statement of Originality

This work contains no material which has been accepted for the award of any other degree or diploma in any university or other tertiary institution and, to the best of my knowledge and belief, contains no material previously published or written by another person, except where due reference has been made in the text.

I give consent to this copy of my thesis, when deposited in the University Library, being available for loan and photocopying.

SIGNED:……..

DATA:……..

Supervisor: Prof. Xiaoyi Bao

Content

List of Figures

List of Tables

List of Acronyms

AOM	Acoustic Optical Modulator
APD	Avalanche Photodiode
BGS	Brillouin Gain Spectrum
BOTDA	Brillouin Optical Time-domain Analysis
CW	Continuous Wave
CWT	Continuous Wavelet Transform
DAQ	Data Acquisition Card
DGD	Differential Group Delay
DOP	Degree of Polarization
DWT	Discrete-Time Wavelet Transform
ECL	External Cavity Laser
EDFA	Erbium-doped Fiber Amplifier
EMI	Electromagnetic Interference
EOM	Electro-Optic Modulator
FBG	Fiber Bragg Grating
FFT	Fast Fourier Transform
FP	Fabry–Pérot
FUT	Fiber Under Test

FWHM	Full-Width-Half-Maximum
GFRP	Glass Fiber Reinforced Polymer
GRIN	Gradient-index
IF	Intermediate Frequency
LPF	Low Pass Filter
NLL	Narrow Linewidth Laser
OFDR	Optical Frequency-Domain Reflectometry
OFS	Optical Fiber Sensor
OTDR	Optical Time Domain Reflectometry
PBS	Polarization Beam Splitter
PC	Polarization Controller
PMD	Polarization Mode Dispersion
PM-PCF	Polarization-Maintaining Photonic Crystal Fiber
POTDR	Polarization Optical Time-Domain Reflectometry
PSF	Polarization-induced Signal Fading
PZT	Lead Zirconate Titanate
SBS	Stimulated Brillouin Scattering
SHM	Structural Health Monitoring
SMF	Single-Mode Fiber
SNR	Signal-to-Noise Ratio

SOP	State of Polarization
STFT	Short Time Fourier Transform
TDM	Time-Division Multiplexing
TLS	Tunable Laser Source
WDM	Wavelength Division Multiplexer
WVT	Wigner-Ville Transform

Chapter 1

1 Introduction

Fiber optical sensor technology has achieved enormous developments and has been widely used in various application areas. The main drive for the fiber sensor research can be attributed to their superior advantages with respect to the conventional method including high sensitivity, compact and lightweight, geometric versatility, immune to electromagnetic interference (EMI) and low cost. A variety of different physical parameters (temperature, strain, vibration, acoustic, magnetic, rotation, etc.) have been successfully measured using different kinds of optical fiber sensing schemes. This thesis aims at developing and constructing distributed optical fiber vibration sensing systems with wide frequency response range and high spatial resolution. The proposed fiber sensor schemes are proved to be able to measure both position and frequency information of the external vibration surrounding the sensing fiber simultaneously, which show a great potential to be developed as a powerful tool for on-site, real-time structural health monitoring.

In this chapter, section 1.1 gives an overview of the research background and motivation for distributed vibration sensors. Section 1.2 presents the research objective and section 1.3 shows a brief outline of the thesis.

1.1 Overview

Structural health monitoring (SHM) has drawn more and more attention in both scientific and engineering field in recent years due to its capability of detecting the internal collapses and failures inside the structures and providing early warnings of structural damages or decays. SHM can be applied on all kinds of infrastructure structures such as dams, tunnels, highways, railways, bridges, pipelines and etc. Generally, a SHM system consists of three major elements: a sensing system, a data processing system (including data collection, communication and storage) and a diagnosing system (including damage detection and retrieval algorithm). The main parameters which the scientists and engineers are interested when interrogating the health condition of the structures are load, deformation, strain, temperature and vibration. Therefore, the specific advantages of optical fiber sensors (OFS) such as lightweight and geometric versatility provide enormous potentials for it to be utilized in SHM system. OFS can be embedded and installed on the existing structures due to its small size. Furthermore, the multiplexing and distributed sensing capability of OFS makes it a desirable choice compared to the conventional methods. Damage identification based upon changes in vibration characteristics of the structures is one of the highly effective non-destructive diagnostic tools for SHM [1-3]. Frequency information is the most important parameter in vibration sensing. For the health monitoring on civil structures and small mechanical structures, the intrinsic frequency can be used to evaluate the structural condition and to identify the internal damages at an early

stage. Vibration sensors with low frequency response [4, 5] are suited for the large structures such as bridges, dams and skyscrapers due to their low intrinsic frequencies. However, for some particular application areas such as crack detection of materials and anomaly detection of engines, the frequency range of these events could be as high as several kHz to MHz. In these cases, the vibration sensors with high frequency response and high spatial resolution are highly desirable in order to prevent potential disasters.

Optical fiber vibration sensors have been greatly developed and exploited due to its application for structural health monitoring and damage detection. It can be either a single-point sensor which only works in a localized region, or it may be a distributed sensor with sensing capability along a length of the optical fiber. Various types of point fiber vibration sensors were proposed and demonstrated based on different kinds of principles and algorithms including fiber Bragg grating (FBG), Fabry-Perot (FP) interferometer and some other novel schemes.

The FBG is a kind of wavelength-dependent optical reflector or filter which is fabricated by introducing a periodic refractive index changes within the core region of the optical fiber [6]. In consequence, a selective reflection occurs at the Bragg wavelength $\lambda_B = 2n\Lambda$, which is depended on the effective refractive index of the grating in the fiber core n and the FBG grating period Λ. Figure 1.1 is a schematic structure of FBG with refractive index profile and spectral response. The basic working principle of FBG-based sensor systems for static measurements is to measure the relative wavelength shift of the reflected "Bragg" signal induced by the measurands such as temperature and strain [7]. For the dynamic

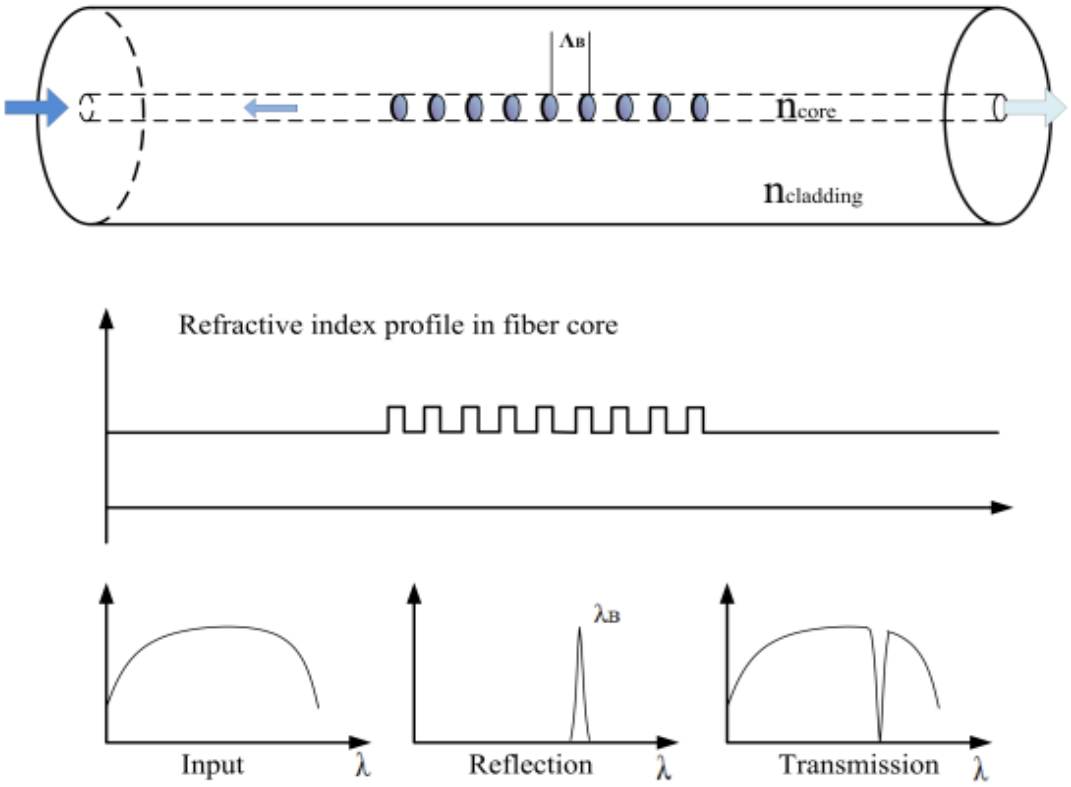

Figure 1.1: Schematic structure of FBG with refractive index profile and spectral response.

sensing case, the vibration signal can be detected by monitoring the intensity modulation of the laser light passing through a FBG attached to a Lead Zirconate Titanate (PZT) vibrator [8]. The sensitivity of the sensor relies on the slope of the FBG transmission spectrum at the operating wavelength. Another vibration sensor based on FBG used an unbalanced Mach-Zehnder interferometer as a wavelength discriminator. The reflected wavelength shift caused by the dynamic strain can be monitored by the output interference signals [9].

Second type of point fiber vibration sensor is based on FP interferometer which can be divided into in-fiber FP interferometry and extrinsic FP interferometer according to the FP

cavity is contained within the transmitting fiber or not. An impact vibration signal was detected by a 10m single mode in-line FP interferometer with 70% end-reflectance placed in a coil on an optical bench in 1982 [10]. Another simple in-line FP interferometer sensor was investigated as an accelerometer with high sensitivity and good linearity. The uncoated cleaved ends of the single mode fiber are used as the reflection mirror to generate the interference fringes[11]. Vibration sensors based on extrinsic FP interferometer have also been developed by many researchers. A simple extrinsic FP interferometer setup with multimode fiber transmission for microdisplacement and vibration sensing was introduced [12]. The FP cavity is formed by the end face of a gradient-index rod (GRIN) lens and a movable reflective surface. The light is coupled into and out of the FP cavity by a pair of multimode fibers. The system is further simplified by a single mode fiber coupler to replace the multimode fiber pair [13]. The results show a dynamic range of 4.29μm at 2 kHz.

Besides the aforementioned methods, a multilongitudinal mode fiber-optic vibration sensor has been presented [14]. The beat frequency between any different longitudinal modes existed in the laser cavity can be modulated by the external vibration because the length of the laser cavity is changed. By using the frequency-modulation demodulation technique, vibration signals up to 20 kHz can be retrieved with high SNR. Another point vibration sensor based on embedded polarization-maintaining photonic crystal fiber (PM-PCF) has been investigated inside a Glass Fiber Reinforced Polymer (GFRP) [15]. The input polarized light is launched into the embedded PM-PCF at 45° to one of the

orthogonal axes so that the two orthogonal polarization modes in the PCF can be excited equally. The application of PM-PCF for vibration sensing is attractive since it is insensitive to the temperature changes.

Distributed fiber vibration sensing has attracted strong research interest due to its unrivalled capability of providing spatial-resolved vibration information along the whole sensing fiber. A wide variety of distributed schemes have been proposed and implemented for dynamic measurement including optical fiber interferometer sensors and optical backscattering based sensors.

A series of interferometer sensors have achieved distributed disturbance detection through the combination of two interferometers together. A merged Sagnac-Michelson interferometer was presented [16]. The input light launched into the Sagnac loop consists of two different wavelengths. A frequency selective mirror in the center of the Sagnac loops reflects one wavelength and transmits the other. A Sagnac interferometer and a Michelson interferometer can be operated at different wavelengths inside the same fiber segment. The position information relative to the mirror can be located by division between the outputs of the two interferometers. A dual-Sagnac interferometer vibration sensor was proposed to detect the disturbance signal in real time [17]. The structure of dual-wavelength and dual-Sagnac interferometer is implemented by using a broadband light source and wavelength division multiplexers (WDMs). A new signal processing algorithm based on the fast Fourier transform (FFT) frequency analysis can help calculate and displaying the position and frequency of the disturbance in real-time. Moreover, a

two-loop Sagnac interferometer is also used for distributed disturbance sensing [18]. The position information is obtained from the two output phase signals of the two Sagnac loops and the amplitude of the perturbation comes from the integration of the phase signal. However, the spatial resolution of this kind of sensor is on the order of tens of meters which are obviously inadequate for high accuracy measurement. Another interferometer method can measure the amplitude and frequency of the acoustic emission and achieve distributed sensing by cascaded configuration[19].

Optical backscattering light including Rayleigh, Brillouin and Raman scatterings is another important approach for realizing distributed sensing. The local external perturbation along the sensing fiber such as temperature, strain, vibration and so on can be detected by the variation in amplitude, frequency, polarization and phase of the backscattering light [20]. Such a measurement could be implemented in both time and frequency domain to access the local information of the interested measurands. The performance of some main distributed fiber sensors based on backscattering light processes is listed in Table 1.1[20]. We can find that the static sensing such as temperature or strain sensing can be accomplished by Raman OTDR or Brillouin systems. Compared to the static measurement which a large number of traces can be used to remove the random noise, the sensor system for distributed vibration requires a fast response time. Dynamic strain measurement based on stimulated Brillouin scattering (SBS) has been reported by using two counter propagating optical pulses [21]. The frequency difference between the pump and the probe pulses are fixed at the half the Brillouin gain spectrum (BGS) instead

of

	Raman OTDR[22]	**BOTDR [23]**	**BOTDA [24, 25]**	**Brillouin Grating[26]**	**Rayleigh OFDR[27, 28]**
Spatial resolution	meter	meter	cm to meter	cm	μm to mm
Sensing range	Tens of km	Tens of km	Up to hundreds of km	Tens of meters	Up to hundred of meters
Measurement time	<3min	1-5min	2-5 min	10+min	(0.01-3)s
Temperature and strain	No	Yes	Yes	Yes	Yes
Temperature accuracy	0.8 °C	2-3 °C	1-2 °C	1 °C	0.1 °C
Strain accuracy	No	60με	20με	10με	1με
Dynamic measurement	No	No	400Hz	No	30Hz

Table 1.1: Performance of different kinds of distributed fiber sensors based on light backscattering.

sweeping the pump-probe frequency difference. The vibration information could be monitored by the power modulation of the probe pulse related to the local Brillouin frequency shift which is induced by the external vibration. The drawback of the above method is that a pre-sweep is required in order to obtain the distribution of the BGS along the sensing fiber. Another simple method for distributed dynamic sensing based on the classical Brillouin optical time-domain analysis (BOTDA) is carried on by fast switching 100 scanning frequencies [29]. The BGS can be obtained on the order of several hundred of microseconds by a digital signal generator. The vibration is detected through the BGS

variation along the time and the frequency response of this method is limited by the number of average. Distributed optical fiber vibration sensor using Rayleigh backscattering has also been studied and implemented by spectrum analysis of the Rayleigh backscattering traces based on the polarization optical time-domain reflectometry (POTDR) system [30]. Changes of the state of polarization (SOP) of the Rayleigh backscattering light induced by the vibration will be converted to intensity variation. By employing fast Fourier transform, the frequency and position information of the vibration can be determined. However, this sort of sensor can only locate beginning point of the vibration events because the backscattered signals after the first disturbing point are contaminated by their previous perturbations.

According to the above discussions, the current fiber vibration sensors have different kinds of shortcomings. Although the point vibration sensor has a high sensitivity, its application is restricted because only the disturbance information within a small range can be accessed. The up-to-date distributed vibration sensors have a poor spatial resolution on the order of tens of meter or a very narrow frequency response around several hundred of Hz. However, some fiber vibration sensor with wide frequency response and high spatial resolution simultaneously for the applications in SHM is not available now. Therefore, the motivation of our research is to develop a distributed fiber optic vibration sensing system with high spatial resolution and wide frequency response.

1.2 Research objective

The objective of the dissertation is to develop the new distributed fiber optical vibration sensors based on Rayleigh backscattering in both time-domain and frequency domain. Furthermore, the detection performance of this kind of new sensors is optimized and improved.

A distributed vibration sensing system based on all-polarization-maintaining configurations of the phase-sensitive optical time domain reflectometry (OTDR) is presented for the first time. Both polarization-induced signal fading and noise are mitigated via polarization-maintaining components. The detectable frequency response is increased to around 2.25 kHz. Moreover, only straight sensing fiber segment of 0.13 m instead of several closed fiber loops is needed to sense the vibration event with a spatial resolution of 1m, which makes it convenient for vibration monitoring in practical applications. The maximum distance between sensing fiber and vibration event can be 18cm.

We proposed and demonstrated a wavelet technique to reduce the time domain noise to get sub-meter spatial resolution in the distributed vibration sensor based on phase optical time domain reflectometry in standard single mode fiber. Wavelet shrinkage denoising approach allows the distributed vibration measurement of 20Hz and 8 kHz events to be detected over 1km sensing length with 5ns optical probe pulse, which is equivalent to 50cm spatial resolution using the single mode sensing fiber.

We developed a new high performance distributed vibration sensor based on time-division multiplexing (TDM) scheme. By setting the time delay between a narrow pules and a quasi-continuous wave properly, conventional phase-sensitive OTDR system

and polarization diversity scheme can be combined together in one single-mode fiber without crosstalk. Position information of the vibration can be determined by the phase-sensitive OTDR system while frequency information is obtained by the polarization diversity schemes. In experiments, a 0.6MHz vibration event is detected with 1m spatial resolution along a 680m single mode sensing fiber.

We also use the continuous wavelet transform (CWT) to study the non-stationary vibration events measured by our phase OTDR system. The continuous wavelet transform approach can give simultaneously the frequency and time information of the vibration event. Frequency evolution is obtained by the wavelet ridge detection method from the scalogram of the continuous wavelet transform. In addition, a novel signal processing algorithm based on the global wavelet spectrum is used to determine the location of vibration. Distributed vibration measurements of 500Hz and 500Hz to 1 kHz sweep events over 20 cm fiber length are demonstrated using a single mode fiber.

Besides the phase OTDR system which utilizes the Rayleigh backscattering traces from the time-domain pulses, the feasibility of optical frequency-domain reflectometry (OFDR) for vibration sensing is also investigated for the first time. The distributed vibration or dynamic strain information could be obtained using time-resolved OFDR. Time-domain information is resolved by measuring Rayleigh backscatter spectrum in different wavelength ranges which falls in successive time sequence due to the linear wavelength sweep of the tunable laser source with a constant sweeping rate. The local Rayleigh backscatter spectrum shift in time sequence could be used to determine dynamic strain

information at a specific position of the vibrated state with respect to that of the non-vibrated state along the fiber length. Standard single-mode fibers (SMF) could be used as sensing head, while the measurable frequency range of 0-32 Hz with the spatial resolution of 10 cm is demonstrated along a fiber length of 17 m.

1.3 Thesis Outline

This thesis consists of eight chapters. An outline of the coming chapters and their main contents is listed as follows:

Chapter 2 presents the fundamental physics of the Rayleigh scattering in optical fiber. Basic principles of OTDR and OFDR based on the Rayleigh backscattering in the fiber are introduced respectively.

Chapter 3 describes a phase-sensitive OTDR system based on all-polarization-maintaining configurations for distributed vibration sensing. The experimental setup and the results of pencil-break event are presented.

Chapter 4 proposes a wavelet denoising method to improve the detection performance of phase- sensitive OTDR system. Comparison between moving average method and this new method is shown in this chapter.

Chapter 5 presents a novel distributed vibration sensor based on time-division multiplexing method for high frequency vibration detection.

Chapter 6 discusses a time-frequency analysis method based on CWT technique for the

measurement of non-stationary vibration event. The frequency evolution with can be determined and a new scheme using the global wavelet spectrum of the CWT for locating the position is also presented.

Chapter 7 demonstrates the feasibility for vibration sensing using time-resolved OFDR. The working principle is illuminated and vibration event can be detected by comparing the spectrum shift of the Rayleigh backscattering light with respect to time.

Finally, chapter 8 gives a summary of the research work we have done and some possible future research topics are discussed.

Chapter 2

2 Principle and applications of Rayleigh backscattering light

Various scattering processes can occur when light travels through matter. Light scattering originates from the fluctuations in the optical properties of a material medium. The light scattering process is referred to as a spontaneous phenomenon if the optical properties of the material medium are not modified by the incident light field [31]. In this case, the fluctuations are excited by thermal effect. In contrast, if the incident light field is intense enough to cause the fluctuations, this kind of light scattering process is defined as stimulated process.

Four types of spontaneous light scattering are schematically shown in Figure 2.1 which include Rayleigh scattering, Brillouin scattering, Raman scattering and Rayleigh wing scattering [31]. The center line without frequency shift is called Rayleigh scattering. It is the scattering of light from nonpropagating density fluctuations, which causes random microscopic variations in the refractive index. It is known as a quasielastic scattering process because there is no frequency shift between the incident and scattered light. Brillouin scattering is represented by the two spectral peaks located on both sides of the Rayleigh scattering. Commonly, the parts of scattering light shifted to the low frequency regions are known as Stokes light, whereas the parts shifted to the high frequency regions

are known as anti-Stokes light. Brillouin scattering comes from the interaction between incident light and sound waves in the medium. It can also be considered to be generated due to the coupling of optical fields and acoustic phonons via electrostriction. The Brillouin frequency shift in optical fiber for the input light at 1550nm is around 11GHz. Another scattering process is Raman scattering which is related to the interaction of light with molecular vibrations, also known as optical phonons in the scattering medium. Both Brillouin and Raman scattering are inelastic processes due to the energy exchanges between light and phonons (acoustic or optical). Rayleigh wing scattering is due to fluctuation in the orientation of anisotropic molecules. The spectrum of this scattering light is very broad because of the rapid process of molecular reorientation. Rayleigh wing scattering does not exist in the optical fiber since the silica molecule is centro-symmetric.

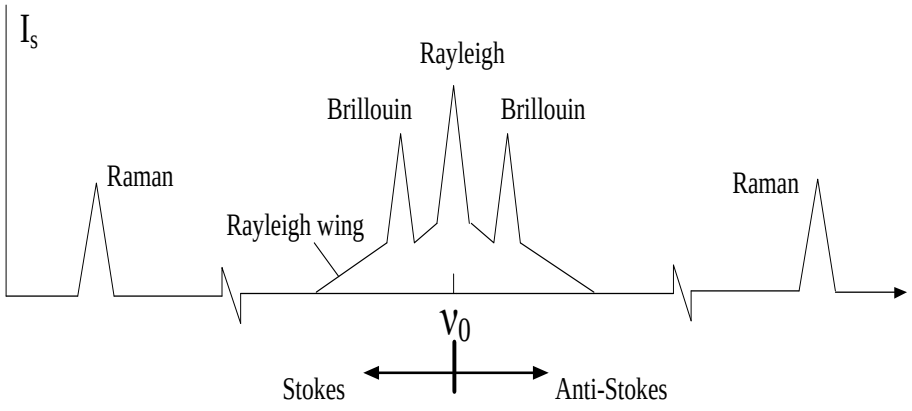

Figure 2.1: Sketch of typical spectrum of light scattering [31]. (Frequency and intensity axis are not scaled to represent the peaks heights and real frequency accurately.)

In this chapter, we will firstly focus on the Rayleigh backscattering in the optical fiber. Then we will discuss the applications of Rayleigh backscattering in optical time-domain

reflectometry and optical frequency-domain reflectometry, respectively. Different kinds of OTDR systems based on Rayleigh backscattering are introduced in section 2.2. The OFDR system utilizing Rayleigh backscattering generated by continuous-wave light (CW) is described in section 2.3.

2.1 Introduction

When a light wave prorogates along an optical fiber, the light power will decrease continuously mostly due to Rayleigh scattering which results from the inhomogeneity of the refractive index during the fiber fabrication process. The random localized fluctuation of the molecule position in the optical fiber can be regarded as small scattering centers with a dimension much smaller than the optical wavelength. The scattered light intensity is inversely proportional to the fourth power of the wavelength λ which means longer wavelengths have lower scattering losses than shorter wavelength. The intrinsic loss of silica fiber from Rayleigh scattering can be expressed as

$$\alpha_s = C / \lambda^4 \tag{2.1}$$

where the constant C is in the range of 0.7-0.9(dB/km)μm^4, depending on the constituents of the fiber core [32].

When an external light field is launched into the fiber, the electromagnetic (EM) field E will rearrange the orientation of the incoherent random fluctuating molecular clouds to respond jointly on a small spatial scale covering a small fraction of the wavelength of the

EM field. This joint response to an EM field will result in macroscopic polarization that is proportional to the external electric field E, $P = \varepsilon_0 \chi E$. ε_0 is the vacuum permittivity and factor χ is a material status dependent quantity symbolizing the joint response. The value χ includes a randomly fluctuating part $\Delta\varepsilon(t,z)$. Therefore a changing polarization-induced light emission in all directions is caused by the variable dielectric parameter $\Delta\varepsilon$. Some of the scattered Rayleigh light is recaptured by the waveguide and guided in the backward direction.

Similar to all of other electromagnetic phenomena, propagation of optical fields in fibers follows the Maxwell's equations. For a nonconducting media like fiber, the Maxwell equations can be written as [33]:

$$\nabla \times \vec{E} = -\frac{\partial \vec{B}}{\partial t}, \quad \nabla \times \vec{H} = \frac{\partial \vec{D}}{\partial t}$$
$$\nabla \cdot \vec{D} = 0, \qquad \nabla \cdot \vec{B} = 0 \tag{2.2}$$

where E and H are electric and magnetic field vectors, respectively. D and B represent corresponding electric and magnetic flux densities. The flux densities are related to the field vectors according to the constitutive relations:

$$\vec{D} = \varepsilon_0(1+\chi)\vec{E} = (\varepsilon + \Delta\varepsilon)\vec{E}$$
$$\vec{B} = \mu_0 \vec{H} + \vec{M} \tag{2.3}$$

where ε is a constant while $\Delta\varepsilon$ describes the locally fluctuating physical mechanism such as spontaneous scattering. Considering Rayleigh scattering $\Delta\varepsilon$ is the variation of the permittivity of the fiber core as a function of time and distance. μ_0 is the vacuum

permeability and $\overrightarrow{M}$ is the induced magnetic polarization which is equal to zero for a nonmagnetic medium like optical fiber.

Combining the Eq. (2.2) and Eq. (2.3), a wave equation of electric field E can be obtained:

$$\mu_0\varepsilon\frac{\partial^2\overrightarrow{E}}{\partial t^2}-\nabla^2\overrightarrow{E}-\nabla[\overrightarrow{E}\cdot\nabla\ln(\varepsilon+\Delta\varepsilon)]+\mu_0\frac{\partial^2(\Delta\varepsilon\overrightarrow{E})}{\partial t^2}=0 \qquad (2.4)$$

The first and second term in Eq. (2.4) represents the ordinary coherent propagation process and the third term is the random spontaneous scattering term caused by the fluctuation $\Delta\varepsilon$. We can assume $\Delta\varepsilon$ to be time independent and replace the partial time derivative of the electric field by $-i\omega$. Then Eq. (2.4) can be simplified as

$$\nabla^2\overrightarrow{E}+\nabla[\overrightarrow{E}\cdot\nabla\ln(\varepsilon+\Delta\varepsilon)]+\mu_0\varepsilon\omega^2(1+\frac{\Delta\varepsilon}{\varepsilon})\overrightarrow{E}=0 \qquad (2.5)$$

In the case of optical fiber, the lateral dependence of the electric field can be ignored and only the longitudinal dependence on z is considered. A scalar differential equation can be obtained:

$$\frac{\partial^2E}{\partial z^2}+\beta^2(1+\frac{\Delta\varepsilon(z)}{\varepsilon})E=0 \qquad (2.6)$$

where $\beta=\omega\sqrt{\mu_0\varepsilon}$ is the propagation constant. One can propose a solution composed of forward and backward traveling wave [27]:

$$E=E_0e^{i\beta z}+\Psi(z,\beta)e^{-i\beta z} \qquad (2.7)$$

Substituting Eq. (2.7) into the scalar differential equation and applying the slow amplitude variation (i.e., $\partial^2\Psi/\partial z^2\cong 0$), we can find:

$$2i\beta\frac{\partial\Psi}{\partial z}-\beta^2\frac{\Delta\varepsilon(z)}{\varepsilon_0}E_0e^{2i\beta z}-\beta^2\frac{\Delta\varepsilon(z)}{\varepsilon_0}\Psi=0 \tag{2.8}$$

For weak Rayleigh scattering over short distances, the following approximation is satisfied:

$$\Psi(z,\beta)<<E_0 \tag{2.9}$$

We can obtain an approximate solution for the backward scattered Rayleigh light due to the random spatial variation of the permittivity:

$$\Psi(z,\beta)-\Psi(0,\beta)\approx\frac{\beta E_0}{2i}\int_0^z\frac{\Delta\varepsilon(\zeta)}{\varepsilon_0}e^{2i\beta\zeta}d\zeta \tag{2.10}$$

$\Psi(0,\beta)$ represents the end face reflection signal, $\Psi(z=L,\beta)$ at most of the case. Therefore the Rayleigh backscattering light is a type of Fourier transform of the random permittivity fluctuation.

Rayleigh backscattering and material absorption are two mechanisms for the fiber loss. Hence, the total attenuation coefficient α (with units of km^{-1}) including scattering coefficient α_s and absorption coefficient α_a can be expressed as:

$$\alpha=\alpha_a+\alpha_s \tag{2.11}$$

Considering the scattering coefficient equals to 0.12-0.16dB/km compared to the attenuation coefficient 0.2dB/km at the wavelength 1550nm, the fiber loss is dominated by Rayleigh backscattering near this wavelength [32] which means that we can roughly estimate the Rayleigh backscattering power from the fiber loss parameters.

The input optical power will attenuate exponentially as a function of the propagating distance *z* as shown in the following equation:

$$P(z) = P_0 e^{-\alpha z} \tag{2.12}$$

where P_0 is the incident light power and *P(z)* is the transmitted power at distance *z*. The attenuation coefficient α is commonly expressed in the unit of dB/km for convenience in practice. Then

$$P(z) = P_0 \cdot 10^{\frac{-\alpha_{dB} z}{10}} \tag{2.13}$$

with $$\alpha_{dB} = \frac{10}{\ln 10} \cdot \alpha \approx 4.34\alpha \tag{2.14}$$

If a laser pulse with peak power P_0 and pulse duration T is injected into one end of the fiber, the Rayleigh backscattering light power dp_{rb} from a small fiber segment can be measured at the same fiber end [34]:

$$dp_{rb}(z) = C_b \cdot \alpha_s \cdot P_0 \cdot e^{-2\alpha z} dz \tag{2.15}$$

where C_b represents the ratio of the total Rayleigh scattered power radiated to all directions that gets captured in the fiber and propagates in the backwards direction. C_b can be expressed as the form [35]:

$$C_b = \left(\frac{NA}{n_1} \right)^2 \cdot \frac{1}{m} \tag{2.16}$$

where $NA = \sqrt{n_1^2 - n_2^2}$ is the numerical aperture, n_1 and n_2 are the refractive index of the core and cladding ,respectively. Factor *m* depends on the refractive index profile of the fiber.

The eq. (2.15) can be rewritten related to *t* by using the relation $2z=v_g t$ as:

$$dp_{rb}(t) = \frac{C_b \cdot \alpha_s \cdot P_0 \cdot v_g}{2} \cdot e^{-\alpha v_g t} dt \tag{2.17}$$

Scattering process at a certain location *z* along the fiber only occur when the laser pulse is passing through. Preforming the integral of eq. (2.17) from *t-T* to *t* we can obtain the formula for the backscattered power $P_{rb}(z)$ [36]

$$P_{rb}(z) = \frac{C_b \cdot \alpha_s \cdot P_0 \cdot T \cdot v_g}{2} \cdot e^{-\alpha z} \tag{2.18}$$

2.2 OTDR based on Rayleigh backscattering

2.2.1 Fundamentals of conventional OTDR system

Conventional OTDR technique based on Rayleigh backscattering inside the optical fiber is firstly proposed to measure the loss distribution along the fiber in a precise and reliable way [37]. Since then this method has become a useful diagnostic tool for monitoring and locating the defects, anomalies and other features of the optical fiber systems during the fabrication, installation and maintenance processes. The basic idea is to launch a short pulse with high power into the fiber under test and measure the time-domain Rayleigh backscattering signals. Figure 2.2 shows a schematic configuration of a conventional OTDR system. The probe pulses generated by a laser source with broad linewidth are injected into the fiber at the input end through an optical circulator or an optical directional coupler. The Rayleigh backscattering light along the fiber travels back to the input port and collected by a photodetector. The electronic signal is amplified and then digitized by data-acquisition card. By using this backscattering method, the fiber losses with the

distance can be estimated and the reflection points caused by the fusion splice and fault can be monitored on the time-domain Rayleigh backscattering traces.

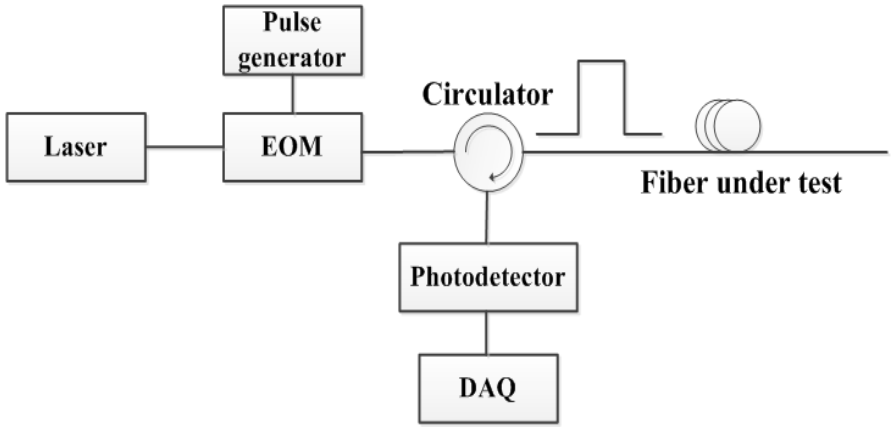

Figure 2.2: Schematic setup of a conventional OTDR

An avalanche photodiode (APD) is typically used in the OTDR system instead of the p-i-n based receiver. The APD detector is well-designed to improve the sensitivity compared to a p-i-n photodetector. The low-band gap semiconductor absorption region inside the APD detector is similar to that of a p-i-n detector. The electrons with high velocity will collide with the lattice in the separate multiplication region to generate more new free electrons, which is called as an avalanche multiplication process. Thanks to its advantage of high sensitivity, the APD detector is able to detect relatively weak optical power such as the Rayleigh backscattering light generated by narrow optical pulses. Bandwidth is one of the important parameters of the APD which can influence the SNR of the OTDR system. The receiver noise is proportional to the detector's bandwidth. Since high spatial resolution requires short probe pulses which correspond to a broader bandwidth to detect the SNR will be deteriorated in this case.

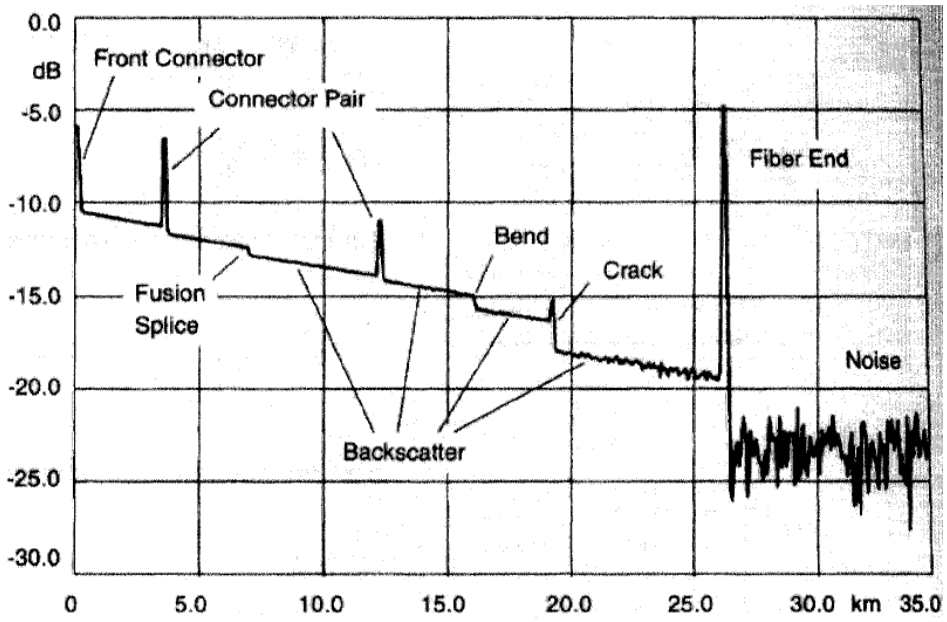

Figure 2.3: Typical OTDR trace [35].

Figure 2.3 presents a typical trace of OTDR measurement. The vertical scale represents the reflected signal level on a logarithmic scale while the horizontal scale corresponding to the distance along the fiber or device under test. Since OFDR can only measures the time delay directly a conversion relation $L = v_g t / 2$ is used to translate to distance from the time.

Three typical types of features exist in an OTDR trace. First is the straight decreasing line representing the Rayleigh backscattering along the fiber. The slope of this line gives the attenuation coefficient of the fiber. Second type is the positive peak corresponding to the connection or crack points with height implying the level of the reflection. The last type is the sudden drop with a step size related to the insertion loss caused by fusion or bending along the fiber. At the end of the fiber, a strong reflection peak is observed determined by the condition of the fiber end surface. Behind this peak no more optical signal can be detected and the OTDR curve decreases onto the noise level depended on the

receiver itself which ultimately limits the performance of the system.

Many parameters are used to evaluate the performance of the conventional OTDR system. Some of the key parameters such as dynamic range, spatial resolution and dead zone are presented here in details. Dynamic range offers the information of the maximum fiber loss than can be detected. It is defined as the difference between the initial Rayleigh backscattering level and the noise floor without optical signal. Two ways can improve the dynamic range of one system, one is to increase the power of the backscattering Rayleigh light and the other is to reduce the noise level. Using probe pulses with high peak power can acquire more Rayleigh backscattering. However, the nonlinear effects such as stimulated Brillouin scattering and stimulated Raman scattering have to be considered and avoided in the high peak power region. Spatial resolution indicates the location accuracy of an OTDR system of resolving the two adjacent events. Its definition based on the pulse width can be expressed as $T_0 v_g / 2$ where T_0 is the pulse width and v_g is the group velocity of the light. Another commonly-used definition for spatial resolution in the area of distributed fiber sensing is 10%-90% rise time of a transition of measurands such as temperature or strain [20]. Dead zone is caused by the reflections that can saturate the receivers in OTDR system. The detector recovers slowly from the overload condition back to the normal condition once it is saturated by strong signals. The returned signal is then superimposed by the receiver's overload process resulting in a loss of information.

Distributed temperature sensing using conventional OTDR system has been investigated by monitoring the temperature induced amplitude changes of the Rayleigh

backscattering light. This kind of temperature sensor has been accomplished in a special liquid-core fiber with an accuracy of $\pm 1^{\circ}C$ and a spatial resolution of a few meters [38]. The liquid-core fiber is fabricated by a glass tube (the cladding) filled with a liquid with higher refractive index to form the fiber core. The temperature dependence of the scattering loss results from the thermal agitation of the liquid so that it has strong temperature dependence. However the requirement of a special fiber instead of standard SMF restricts its real application. Another temperature sensor based on conventional OTDR utilizes the temperature dependence of the attenuation coefficient of doped glass fibers. The absorption bands of the dopants will shift with temperature. Temperature changes can be determined by measuring the loss near the edge of an absorption band. Distributed temperature measurement using Nd doped fiber showed $2^{\circ}C$ temperature accuracy and 15m spatial resolution over 140m sensing fiber length [39].

OTDR systems based on coherent detection scheme has also been proposed [40, 41] and used for achieving high performance with respected to direction detection. However, the returned Rayleigh backscattering time-domain trace will appear a jagged profile when a narrow linewidth laser source is utilized to generate the probe pulse [42]. This jagged appearance is due to a speckle-like phenomenon caused by the coherent addition of a lot of scattered light in the reversed direction within the pulse width. In the direct detection case, the spectral width of the modulated laser is usually very broad on the order of GHz to THz so that this phenomenon can be avoided because the interference effect of the Rayleigh backscattering light is not strong enough. Moreover, the shape of the returned traces may

vary from pulse to pulse due to the fluctuation of the laser frequency. The amplitude variation of the traces will affect the accuracy of the optical loss measurement obtained by a coherent OTDR and cause a deterioration of signal-to-noise-ratio (SNR). Some techniques have been demonstrated to reduce this influence [43, 44].

2.2.2 Fundamentals of phase OTDR system

In contrast, the phase-sensitive OTDR system is designed to utilize the interference effects within the narrow probe pulses by using a laser source with narrow linewidth and stable frequency. The phase-sensitive OTDR for distributed intrusion sensing was proposed by reported firstly by Henry F. Taylor [45, 46]. Figure 2.4 shows the setup of phase-sensitive OTDR used for distributed intrusion sensing. The configuration of phase-sensitive OTDR is quite similar to the conventional OTDR system except the laser source. A light source with narrow linewidth and minimum frequency shift is selected. Probe pulses are generated by an intensity modulator such as electro-optical modulator (EOM) and launched into the sensing fiber through an optical coupler. The electric signals from the photodetector represent the amplitude of the Rayleigh backscattering light along the fiber. Assuming that both the sensing fiber and the laser source are stabilized which means that the statistical feature of Rayleigh scattering along the fiber length could be considered to be not changed, the time-domain traces will show a unique signature due to the interference effect. If a certain section of the sensing fiber is under external

disturbances caused by intruders, the refractive index or length of the fiber will be varied. As a consequence, the Rayleigh backscattering light at the perturbed region will experiences an extra phase shift compared to the stable state. The intensity of the interference from Rayleigh scattering centers within the pulse width will be changed. The intrinsic characteristic of the time-domain traces is also different from the case without intrusions. Position information of the intrusions can be determined by an appropriate detection algorithm.

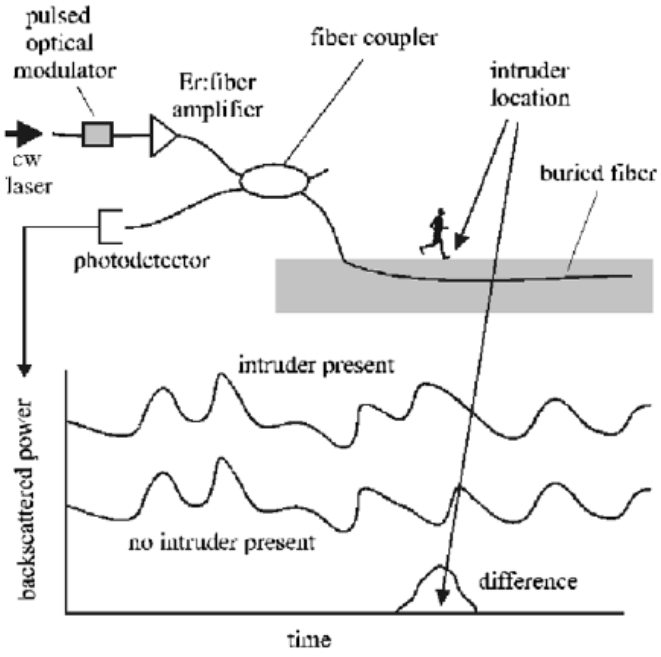

Figure 2.4: Phase-sensitive OTDR used for intrusion sensing [46].

In order to investigate the feasibility of the phase-sensitive OTDR, a simple discrete model for simulating the interference effect of Rayleigh backscattering in an optical fiber has been proposed [47]. As shown in Figure 2.5, a fiber with length L is divided into N small sections and the size for each section $\Delta L=L/N$. Rayleigh backscattering process in

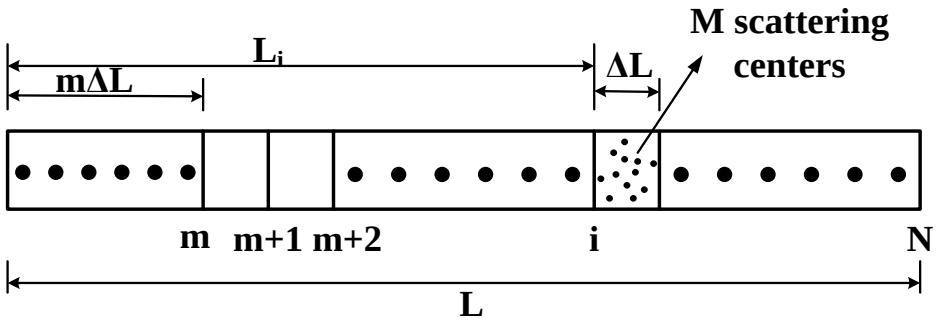

Figure 2.5: Diagram of the discrete model of Rayleigh backscattering in optical fiber

the optical fiber can be represented by a set of N discrete reflectors. The i^{th} reflector can be regarded as the coherent addition of randomly distributed scatters within one small section ΔL. The number of scattering centers in ΔL is set to be M. Hence, the interference field of Rayleigh backscattering light at distance L_i can be expressed by

$$\vec{E}_b(L_i) = E_0 e^{-\alpha(i-1)\Delta L} \sum_{k=1}^{M} a_k^i e^{j\varphi_k^i} \tag{2.19}$$

where E_0 is the electrical field of the incident light, α is the attenuation coefficient of the fiber, and a_k^i and φ_k^i represent the amplitude and the phase of the k^{th} scatter center in i^{th} section, respectively. This expression indicates that the interference among the Rayleigh backscattering light can be represented by the complex sum of the amplitude and phase of the scattering centers in one section.

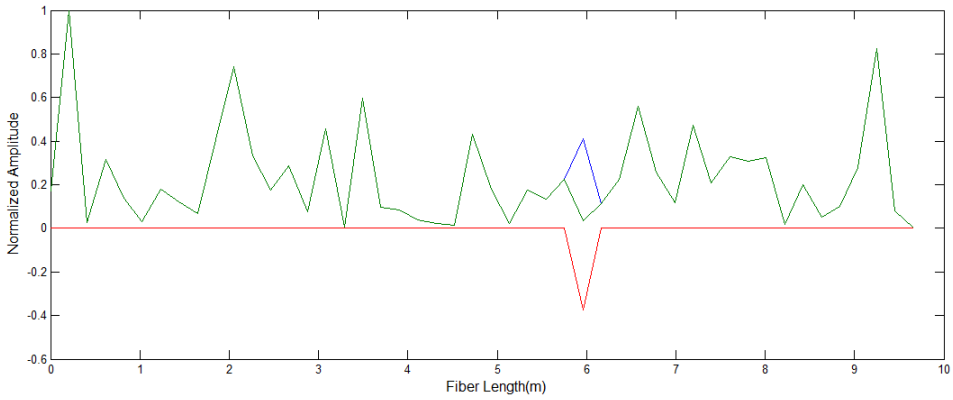

Figure 2.6: Simulated time-domain Rayleigh backscattering traces along the sensing fiber. (Small peak on the red curve represents the difference between two traces caused by external disturbance).

A simulation result of the jagged time-domain Rayleigh backscattering traces is shown in Figure 2.6. The sensing fiber length is 10m and the length of each fiber section is 10cm. Since the size of Rayleigh scattering center is comparable to the wavelength, the number of scattering center is chose to be 10000 in each fiber section. In Figure 2.6, the green solid curve represents the time-domain trace without disturbance and the blue dashed line which is covered by the green curve, shows the case under the disturbance. It is hidden behind the green curve because the two traces are the exactly same except for the fiber region under the disturbance that the Rayleigh backscattering signal is modulated by the disturbance. Bottom red curve is the subtraction between the two raw traces which clearly shows the position information of the external disturbance.

2.2.3 Fundamentals of polarization OTDR system

As we discussed in the previous sections, conventional OTDR only employs the

information contained in the intensity of the Rayleigh backscattering light. Polarization OTDR is one kind of extension of the conventional OTDR by monitoring the spatial distribution linked to the local polarization state of Rayleigh backscattering light [48, 49]. The local SOP can be modulated by the external disturbance such as temperature, strain, pressure as well as electric and magnetic fields. However it is challenging to distinguish these parameters since all of them can cause the polarization change.

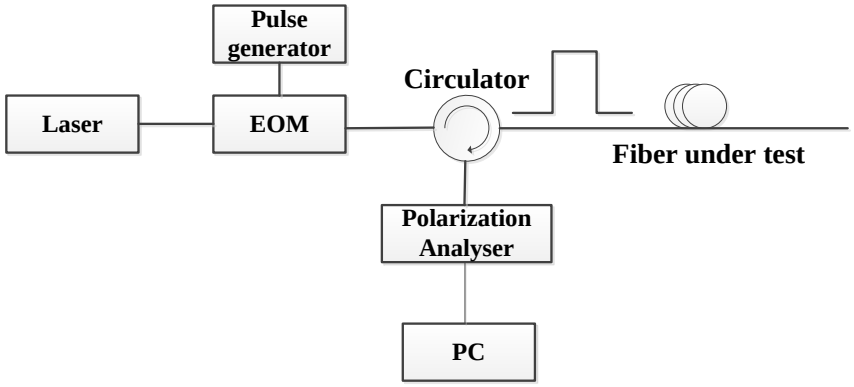

Figure 2.7: Typical experimental configuration for polarization-OTDR

The basic experimental setup is presented in Figure 2.7. CW light wave emitted from a laser source with broad linewidth around 0.1nm passes through an EOM to generator narrow and intense pulses. The pulses are launched into the fiber under test by an optical circulator and the Rayleigh backscattered light is collected by a polarization analyser in order to acquire the strokes components. The SOP distribution along the fiber under test can be obtained and interested measurands can be derived by analyzing the SOP changes.

Measurements of birefringence induced by bending [50] and twisting [51] in single mode fiber have been demonstrated using POTDR technique. In addition, it can also be

used to extract the intrinsic local birefringence in a single-mode fiber by acquiring three POTDR traces using a rotary linear polarizer [52]. Due to its capability of evaluating the birefringence evolution with distance, POTDR offers a new method for polarization mode dispersion (PMD) measurement. PMD is a major factor in limiting the transmission rate in high speed optical fiber communication system due to the pulse broadening. PMD compensation is very difficult to achieve because it is a random process and it evolves with time [53]. High PMD commonly only exists in one or a few small bad regions along a long fiber cable due to the fabrication process or local environmental changes such as temperature gradient, strong wind and etc. [54]. Therefore a technique which can assess the PMD distribution effectively will be valuable. PMD characterization using wavelength scanning POTDR has been implemented by measuring the differential group delay (DGD) directly along fiber under test with a tunable laser source [55]. PMD can also be inferred by two physical parameters, the beat length and the coupling length by measuring the degree of polarization (DOP) of the backscattered pulse [56].

2.3 Optical frequency-domain reflectometry

2.3.1 Working principle

Conventional OTDR technique can achieve a sensing length of tens of kilometers with a spatial resolution on the order of meter. In contrast, optical frequency-domain

reflectometry can interrogate the fiber under test with spatial resolution less than 1mm along a fiber up to 2km [57]. The idea of frequency domain reflectometry was proposed for electric radar firstly about half a century ago [58] and then introduced into the optics field for the first time in 1981 [59]. A schematic configuration of the classical OFDR system is shown in Figure 2.8. Instead of launching probe pulses into the sensing fiber in OTDR case, probe light from a highly coherent tunable laser source whose optical frequency can be scanned continuously in a time-linear sweep is utilized for OFDR system. The coherent Rayleigh backscattering light is mixed with the light from reference arm (also called local oscillator) at a photodetector. Assuming a position l along the sensing fiber, the corresponding round-trip transmit time τ of the Rayleigh backscattering light is

$$\tau = \frac{2l}{v_g} \tag{2.10}$$

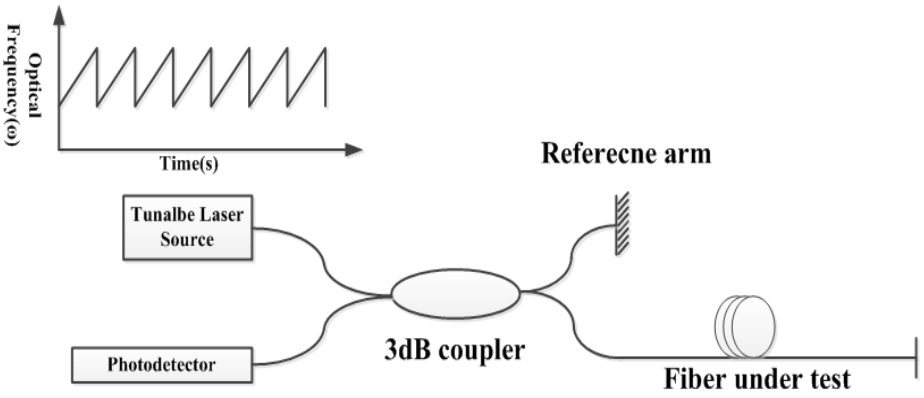

Figure 2.8: Schematic setup of a classical OFDR system

where v_g is the group velocity of light inside the fiber. Define the optical frequency sweep rate $\gamma = d\omega / dt$, and then the optical frequency change Ω during the transmit time can be expressed as [59]

$$\Omega = (\frac{2l}{v_g}) d\omega / dt \tag{2.20}$$

This frequency component is carried by the returned backscattering signal. Its frequency value represents the position information along the fiber and its amplitude is proportional to the local backscattering factor. By performing a fast Fourier transform (FFT) on the raw signals collected on the detector, OTDR-like traces including the Rayleigh backscattering light distribution along the fiber will be obtained. A detailed theoretical derivation to explain the basic principle of the OFDR is discussed in the following part.

The amplitude of the electric field at position $l = 0$ along the fiber of length L can be assumed as E_0. The forward propagating electric field can be expressed as $E(l)\exp(i\beta l)$ along the fiber where β is the propagation constant and the real amplitude $E(l) = a^{1/2} E_0$ with attenuation function[59]

$$a(l) = \exp\left[-\int_0^l \alpha(\xi) d\xi \right] \tag{2.21}$$

The contribution of a small fiber segment dl with a localized scattering coefficient $\sigma(l)$ to the total backscattering light emerged from the whole fiber under test is $E(l)\sigma(l)dl$. The overall Rayleigh backscattering amplitude can be written as [59]

$$E_S(\beta) = E_0 \int_o^L \sigma(l) a(l) \exp(2i\beta l) dl \tag{2.22}$$

As the requirement of the OFDR principle, the spatial frequency β should be swept linearly with a form: $\beta(t) = \omega(t) / v_g = \beta_0 + \mu t$ where $\mu = (1 / v_g) d\omega / dt$ is the sweep rate.

In coherent detection scheme, a reference arm with higher amplitude value is produced

by a reflection of the forward propagating lightwave with a known amplitude reflection coefficient r at a carefully chosen reference position l_r. Therefore the expression of the reference field can be written as [59]

$$E_R(\beta) = rE_0 a(l_r)\exp(2i\beta l_r) \tag{2.23}$$

Then the optical intensity associated with the interference between the Rayleigh backscattering wave and the local oscillator light can be given by

$$\begin{aligned} I(\beta) &= \left|E_S + E_R\right|^2 \\ &= \left|E_S\right|^2 + \left|E_R\right|^2 + E_S(\beta)E_R^*(\beta) + E_S^*(\beta)E_R(\beta) \\ &= \bar{I} + \tilde{I}(\beta) \end{aligned} \tag{2.24}$$

In the above equation, the DC portion $\bar{I}$ can be ignored because it is independent on the propagation constant β. Only the AC term $\tilde{I}(\beta)$ which is related to β will be considered in the following discussion. We can define $g(\beta) = E_S(\beta)/E_R(\beta)$ as the normalized Rayleigh backscattering signal. Combining eq. (2.13) and (2.14) we can obtain [59]

$$g(\mu t) = \int_0^L G(l)\exp\left[2i(l-l_r)\mu t\right]dl \tag{2.25}$$

$$G(l) = \left[\sigma(l)a(l)/ra(l_r)\right]\exp\left[2i\beta_0(l-l_r)\right] \tag{2.26}$$

The above equations tell us that the distribution of the normalized Rayleigh backscattering signal g along the fiber is related to the angular frequency $\Omega = 2\mu\left|l-l_r\right|$. This angular frequency is the beating frequency of the signals from the measurement arm and the reference arm at position l and l_r respectively. We can assume that the reflector is located at one end of the fiber and then the maximum angular frequency $\Omega_{\max} = 2\mu L$

which is corresponding to the backscattering signal at the other end of the fiber. Therefore, each position l can be represented by a special angular frequency Ω. Due to this correspondence between position l and angular frequency Ω, the spatial information $G(l)$ can be calculated by $G(\Omega)$. By performing inverse Fourier transform on eq. (2.16), the desired spatial information $G(\Omega)$ which is equivalent to $G(l)$ can be expressed as [59]

$$G(\Omega) = \frac{1}{2\pi}\int_{-\infty}^{+\infty} g(\mu t)\exp(-i\Omega t)dt \qquad (2.27)$$

2.3.2 Applications of OFDR system

Typically, OFDR offers advantages over OTDR for certain applications that require a combination of high sensitivity and high spatial resolution over intermediate length regions. It has been developed as a powerful technique for characterization of fiber-optic component and device [28, 60-63], distributed optical sensing [27, 64], and biomedical imaging [65]. Recently, a polarization diverse OFDR system has been proposed to achieve a highest reported combination of sensing length (35m) and spatial resolution (22μm) with a very high sensitivity [28]. Polarization diversity scheme is used in this novel OFDR to avoid the signal fading induced by the mismatch of the state of polarization state between the measurement and local oscillator field. Figure 2.9 gives a demonstration of the spatial resolution obtained by the OFDR measurement of the reflectivity of two slightly mismatched fiber PC terminations. The separation between two peaks is 100μm. The

spatial resolution of the system is defined as the full-width-half-maximum (FWHM) of the individual peaks which is around 22μm.

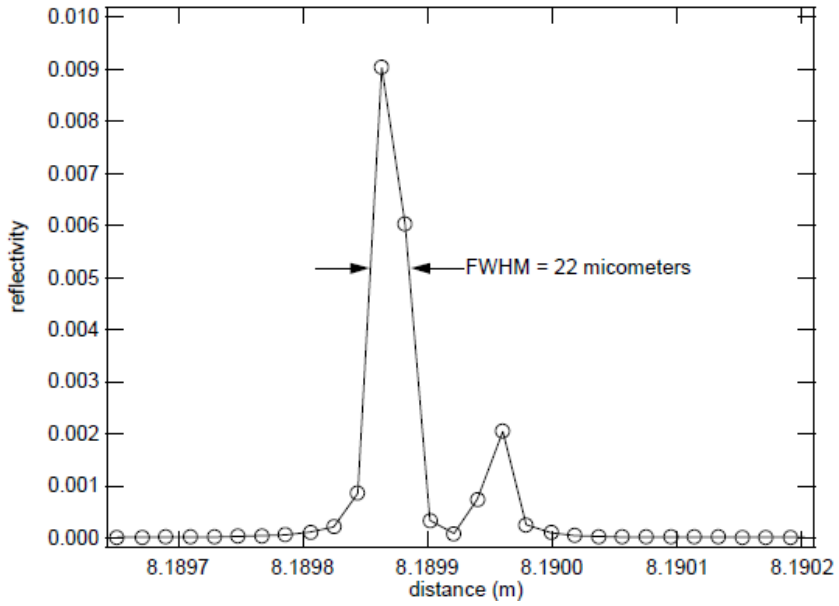

Figure 2.9: Demonstration of the spatial resolution of the OFDR system by using two slightly mismatched fiber PC terminations [28].

Furthermore, researchers from Luna Technology extended the application of OFDR to the optical sensing field [27]. The Rayleigh backscattering induced by the random fluctuations of the refractive index inside the fiber core can be modeled as a Bragg grating with a random variation of amplitude and phase. The response of the Rayleigh backscattering spectrum within a certain wavelength range will keep constantly as long as the sensing fiber stays in a stable state. There will be an overall spectrum shift of the Rayleigh backscattering light if the parameters of the surrounding environment changes such as temperature or strain. This temperature or strain dependent spectrum shift hidden in the random and complex Rayleigh backscattering spectrum can be determined by the mean of

cross-correlation between reference scan and measurement scan (heated or stretched). Figure 2.10(a) shows the Rayleigh backscattering spectrum of a 5mm fiber segment for a reference scan at room temperature and scan of the same fiber interval after heating. The overall shift of the spectrum is obvious but the exact value of spectrum shift is difficult to be determined directly from the two curves of spectrum. Figure 2.10 (b) presents the cross-correlation results between the reference scan and the scan under temperature change. The temperature shift in this fiber section is directly proportional to the wavelength shift corresponding to the peak shift.

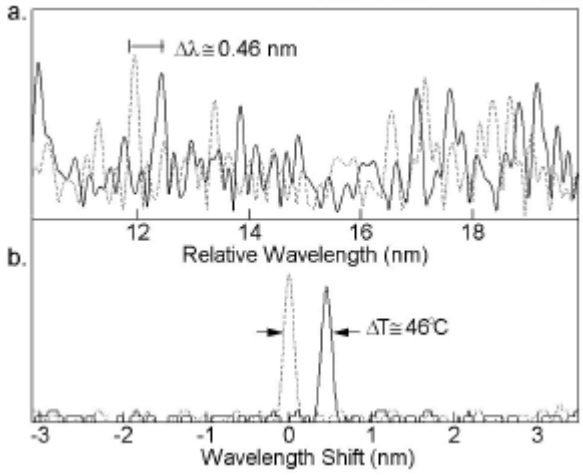

Figure 2.10: a. Rayleigh spectrum along a 5mm fiber section for a heated (solid) and unheated (dotted) measurement scan. b. Cross-correlation of the heated spectrum with reference spectrum [64].

In addition to above applications, recently OFDR has been used to measure the distributed mode coupling along tapered single-mode fibers [66]. The relation between the wavelength shift and the refractive index difference at position z of different modes is expressed as [66]:

$$\Delta n_{ij} = \frac{n_i}{\lambda_i} \Delta \lambda_{ij} \tag{2.28}$$

where $\Delta \lambda_{ij}$ is the wavelength difference between two modes , λ_i and n_i are the wavelength and refractive index for the i^{th} mode ,respectively ,and $\Delta n_{ij} = \left| n_i - n_j \right|$. Therefore, the single-mode and multimode regions of the tapered fiber are characterized and the refractive index difference between the fundamental mode and high order modes of the taper can be calculated by using autocorrelation data processing.

Chapter 3

3 High sensitivity distributed vibration sensor with polarization-maintaining configurations of phase-OTDR

Phase-sensitive OTDR has been successfully applied for distributed intrusion sensing due to its distinguished feature. The method is proved to be a power tool for weak disturbance detection because of the high sensitivity induced by the interference effect of the Rayleigh backscattering light. Our group further extended this method into another important and attractive application field: distributed vibration sensing. A distributed vibration sensor by using heterodyne detection and moving averaging method for the phase-sensitive OTDR has been developed [67]. Vibration events induced by both pencil-break and PZT have been tested in a way that both the position and frequency information can be monitored simultaneously. However, the detection performance of this system such as spatial resolution and frequency response range is not as good as enough to meet the requirements for a real application.

In this chapter, we propose a distributed vibration sensor based on the polarization-maintaining fiber (PMF) configuration to increase detection sensitivity in frequency response, and better spatial resolution, as well as shorter vibration interaction length. As a result, the state of the polarization (SOP) remains constant throughout the

sensing fiber and system configuration; hence the intensity fluctuation noise induced by polarization change is reduced. A 0.13m straight-line PMF is used to replace the previous 0.5m long SMF loops, which removed the pre-knowledge requirement on the vibration event location, and this brings the current sensor configuration a step closer to practical applications for structural health monitoring. Experiment results show that the maximum detectable frequency of PMF has been increased to around 2.25 kHz. The maximum distance between the sensing fiber and the vibration event can be 18cm. Moreover, the spatial resolution has been improved from 5m to 1m. Section 3.1 gives a brief description about the working principle of polarization-maintaining fiber and some applications. The experimental setup based on all polarization-maintaining components is introduced in section 3.2. The experimental results of pencil-break event test are presented in section 3.3.

3.1 Overview of polarization-maintaining fiber

The fundamental mode (TEM_{00}) in an ideal standard single-mode fiber with a perfectly cylindrical core of uniform diameter is a degenerate combination of two orthogonal polarization modes. However, the two orthogonal polarization modes will not keep degenerate and the fiber shows a property of birefringence due to nonuniformity in the shape of the fiber core along the fiber length in the real fibers during the manufacture process. The degree of modal birefringence is defined by [32]

$$B_m = \left| \bar{n}_x - \bar{n}_y \right| \tag{3.1}$$

where $\bar{n}_x$ and $\bar{n}_y$ are the mode refractive indices for the two orthogonal polarization fiber modes. Furthermore, a periodic power exchange between the two polarization modes due to birefringence will occur. The period, which is commonly termed as beat length, is expressed by

$$L_B = \lambda / B_m \tag{3.2}$$

In conventional single-mode fibers, birefringence does not stay constantly but varies randomly along the fiber length in both amplitude and direction due to the nonuniformity of the core shape. A light launched into this kind of fiber with linear sate of polarization will experience a random change of SOP and reach an arbitrary state of polarization.

In order to preserve the state of polarization when light travels inside the fiber, a much higher birefringence needs to be introduced by modifying the structure of the fiber. Polarization-maintaining fiber (PMF or PM fiber) is one kind of special fibers in which the state of polarization of the linearly polarized light can be maintained if it is launched to fast axis or slow axis. The basic idea of PMF is to induce a strong internal birefringence via the stress-rods within the cladding regions. Cross-coupling of the optical power between the two orthogonal polarization modes can almost be prevented by the internal birefringence. Figure 3.1 shows cross-section profiles of two commonly-used PMF: Panda and Bow-tie.

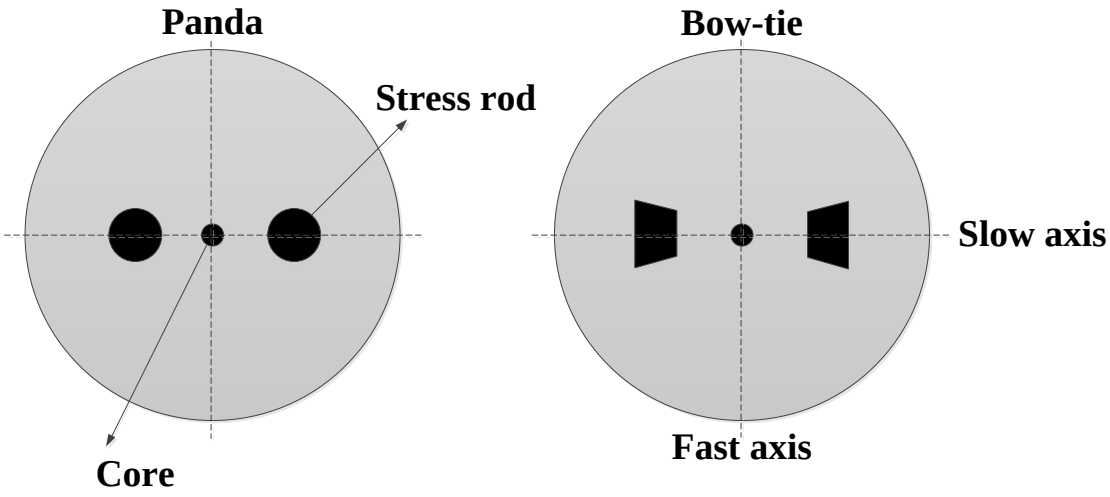

Figure 3.1: Cross-section profiles for Panda and Bow-tie types of polarization-maintaining fiber.

They are different from each other according to the shape of the internal stress-rods which is two circles for Panda type and two bow-ties for bow-tie type. PM fiber has found many specialized applications in both telecommunication fields and optical fiber sensing areas. It is widely used for the connection between a laser source and an intensity modulator in telecommunication because input light with linear SOP is necessary for the modulator. Strain and temperature discrimination for distributed sensing has been presented by using PM fiber in OFDR system [68]. The difference in the refractive index between the two polarization modes is temperature dependent but only weakly influenced by external stain due to the large residual stresses induced to the fiber during the PM fiber fabrication process. By observing the side peak shift in the auto-correlation spectrum and central peak shift in the cross-correlation spectrum of the Rayleigh backscattering light, both strain and temperature can be measured simultaneously. Another promising application is Brillouin dynamic grating generated inside PM fiber [26]. The acoustic

waves induced by the stimulated Brillouin scattering (SBS) on one axis of the PM fiber can be considered as moving gratings for the reflection of the pump wave. By measuring the spectrum of this moving grating on the other axis using a probe pulse, distributed birefringence measurement, as well as discrimination of temperature and strain, can be achieved [69, 70].

3.2 Experimental setup

The coherent phase-OTDR system, like other interferometric fiber-optic sensors constructed using the low-birefringence single-mode optical fiber and fiber components, typically exhibits signal fading problem due to the random fluctuations in the state of polarization (SOP) of the two interference beams. This signal fading problem leads to more moving averaging time to reach a given signal to noise ratio (SNR). Several schemes have been proposed to overcome polarization-induced signal fading (PSF), for instance, polarization masking technique [71] and polarization diversity detection method [72].

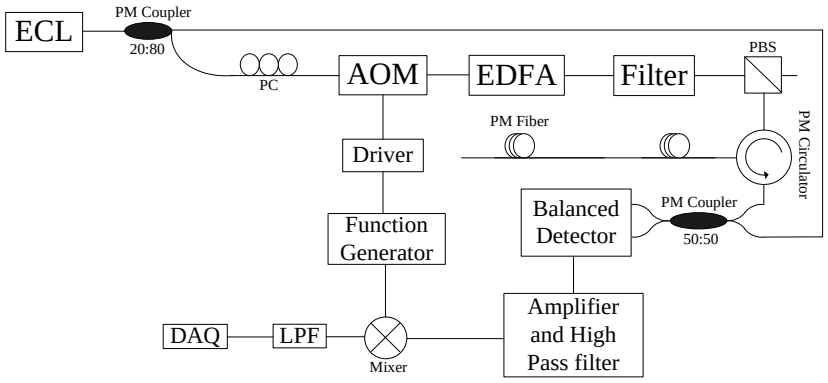

Figure 3.2: Experimental setup for coherent phase-sensitive OTDR based on polarization-maintaining configurations, AOM: acoustic optical modulator; PC: polarization controller, Filter: optical fiber grating filter; LPF: low pass filter; DAQ: data acquisition card.

The experimental setup of the phase-sensitive OTDR based on a polarization-maintaining configuration is shown in Figure 3.2. The light source is an external cavity laser (ECL) with narrow linewidth of 20 kHz and low frequency shift of less than 5MHz. The output wavelength of the ECL is 1548.27nm and the maximum output power is ~10mW. The CW light with a linear polarization state from the ECL is split into two parts by an 80:20 polarization-maintaining coupler. The pulses with a 10 kHz repetition rate and a 200MHz frequency shift induced by an acoustic-optic modulator (AOM) are amplified by an Erbium-doped fiber amplifier, and then the ASE noise is filtered by using an optical fiber Bragg grating. The pulse width is adjusted to 50ns. The filtered pulses with a linear polarization can be generated by a polarization beam splitter (PBS) because the PBS can split the input light into two orthogonal linear polarization states. The linear polarization pulse from one port of the PBS is launched into one principal axis of the PM sensing fiber by a polarization-maintaining circulator. Another part is used

as a local oscillator which is combined with backscattered Rayleigh signal from fiber under test via a circulator by a 3dB polarization-maintaining coupler. The states of polarization of both the local oscillator light and the backscattered Rayleigh light can be preserved linearly using polarization-maintaining fiber components.

3.3 Experimental results and discussions

3.3.1 Fiber layout for pencil-break event measurement

We use the pencil-break on a thin aluminum plate as the vibration source. Pencil-break measurement is a standard technique to emulate the acoustic emission of cracks in concrete or steel bridges for early crack identification. In our previous work [67], we use the fiber loops shown in Figure 3.3(a) glued on the aluminum plate in order to enhance the signal since the noises exist in the system. This kind of layout actually is difficult to be installed and embedded in the infrastructure. Instead of fiber loops, a 0.13m straight fiber located around 95m along a 100m sensing polarization-maintaining fiber was glued to a thin aluminum plate (1mm thickness) by using silicone, shown in Figure 3.3(b). Compared to the fiber loops, the straight line layout suits better for the practical situation. Pulsed elastic surface waves are produced by breaking an HB2 pencil lead on the surface of the aluminum plate. The pencil lead was broken at 1cm from the sensing fiber. The pulsed signal generated in the test plate by the pencil-break is an impact signal, so its frequency

components are broadband frequency event from tens of Hz to several MHz depending on the elastic property of the aluminum plate, and the thickness of the plate.

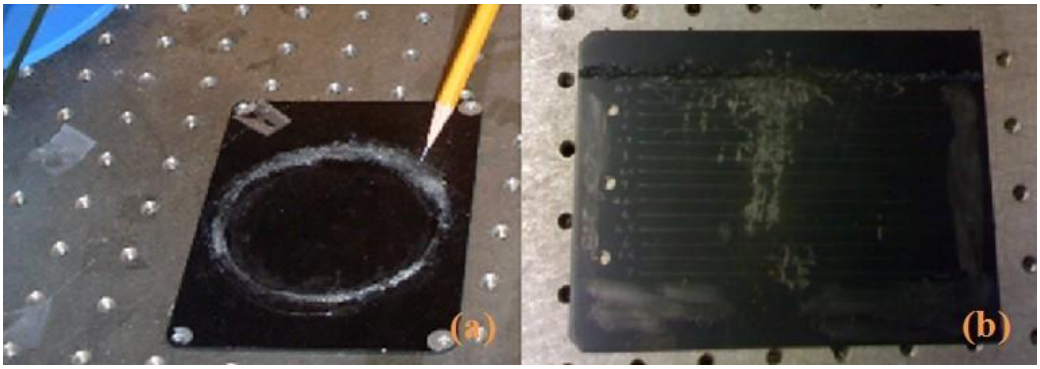

Figure 3.3: Fiber layout for pencil-break event measurement: a. fiber loops, b. straight fiber.

3.3.2 Moving average and moving differential method

In order to reduce the amplitude fluctuation in Rayleigh signal traces due to phase noise of the laser, partial interferometric problem (random polarization), and electrical noises such as thermal noise and shot noise, moving average and moving differential methods are proposed to analyze the raw traces and to determine the location information of the pencil-break event. Supposed that there are N raw traces set $r=\{r_1,r_2,r_3,...r_i...,r_N\}$, where r_i means the i^{th} raw trace. Here raw trace means the trace was directly acquired by using DAQ card for all probe pulses. If moving averaging number is M, the averaged traces set is $R=\{R_1,R_2,R_3,...R_i...,R_K\}$,where $K=N-M+1$; and [67]:

$$R_i=\frac{1}{M}\sum_{l=i}^{l=i+M-1} r_l \quad l\in[1,N], i\in[1,N-M+1] \tag{3.3}$$

The location information cannot be obtained by comparing the adjacent traces of the new

traces *R* because they are very similar. Considering the pulse duration time and the decay time of pencil-break vibration, we choose $R_r = R_{\mathrm{int}(i/2M)\times M+1}$ as the moving references, and then the differential traces could be obtained by following scheme：

$$\Delta R = \{\Delta R_1, \Delta R_2, ..., \Delta R_i, ..., \Delta R_J\} \tag{3.4}$$

where $\Delta R_i = R_i - R_r$, $J = K - 1 = N - M$. The purpose of moving averaging method is to use much more similar traces to reduce random noise in the limited raw traces, and the advantage of moving differential method is to get the detailed difference among the averaged traces because adjacent two averaged traces are too similar to get the difference.

3.3.3 Experimental results for pencil-break events

In our experiment, the pulse repetition rate is 10 kHz that is limited by the maximum trigger frequency of the DAQ-card and the pulse width is set at 50ns. 1000 backscattered traces are acquired for one pencil-break event detection. Figure 3.4 shows the traces for a moving average time of 100. We can clearly observe the amplitude changes among different traces due to the pencil-break event around 140 meters. For other fiber regions without external disturbance, the amplitude almost keeps the same after the random noises are removed.

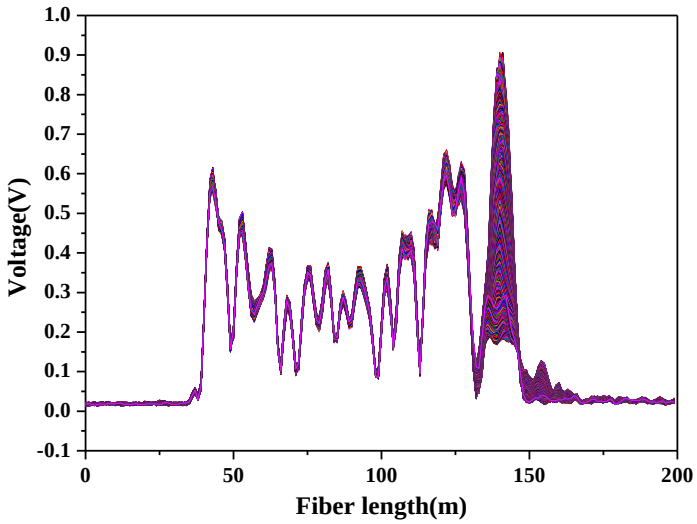

Figure 3.4: Time-domain Rayleigh backscattering traces after 100 moving average time for pencil-break event detection with 50ns pulse width.

The pencil-break location is shown in Figure 3.5 (a), (b), (c) by the moving differential method under different moving averaging times of 4, 10 and 100 respectively. Figure 3.5 (a), (b), (c) includes all the traces after the moving differential method and the inset figures show the moving differential results of two typical traces. Here we define the SNR as a voltage ratio between the mean voltage of the backscattered Rayleigh signal and the mean noise floor $SNR = 10\log(V_{Rayleigh} / V_{noise})$. The result with a SNR larger than 2dB can be regarded as a detectable signal. Experiment results show that at least 4 moving average are needed to obtain a detectable signal compared to the setup constructed using the single-mode fiber components which 10 average times is needed. The location of the pencil-break can be observed with a SNR around 2.2dB. The noise level can be further reduced as the average time increases, so does the SNR improvement. For an average time of 100, the SNR can be as high as 7.6dB.

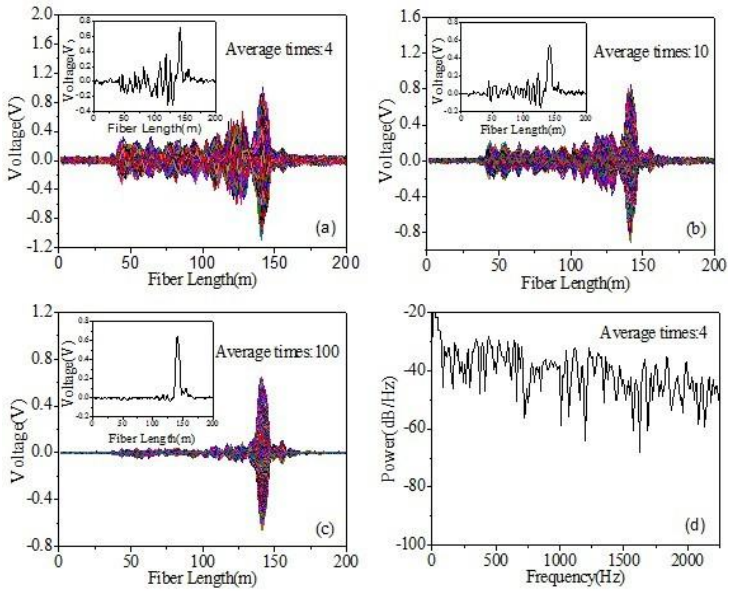

Figure 3.5: Pencil-break detection with 50 ns pulse (the circled part means the location of vibration): (a), (b) and (c) location information by differential method for different averaging times of 4, 10 and 100; (d) power spectrum for averaging times of 4, in which the maximum detectable frequency is 2.25 KHz

Figure 3.5 (d) is the power spectrum of a pencil-break event for averaging times of 4. We find the maximum frequency response is increased to 2.25 kHz because the moving average time is decreased. Although the pencil-break event comprises broad frequency components, we can only get partial frequency components due to the limitation of the pulse repetition rate at 10 kHz determined by the maximum trigger rate of our data acquisition (DAQ) card. More frequency information can be obtained when a DAQ-card with higher trigger rate is used.

The performance of the system under narrow pulse with 10ns pulse duration is tested. The location information and power spectrum under moving average time 4 are shown in Figure 3.6 (a) and (b) respectively. It shows that the spatial resolution can be reduced to

1m with the same measurable frequency range.

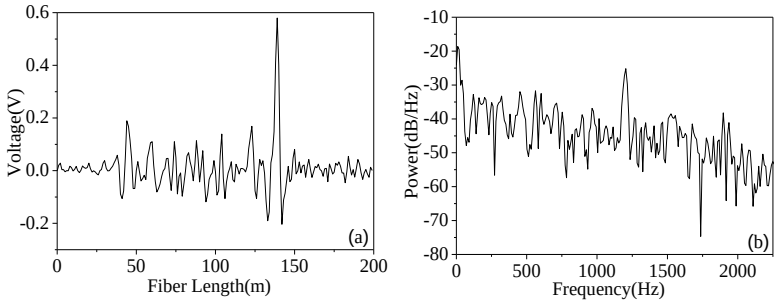

Figure 3.6: Pencil-break detection with 10 ns pulse: (a) location information under moving average times 4; (b): power spectrum for averaging times of 4

Figure 3.7 gives the simultaneous measurement of two pencil-break events at different positions. The position information at every point shows the capability of the phase-sensitive OTDR for distributed sensing with PMF configuration.

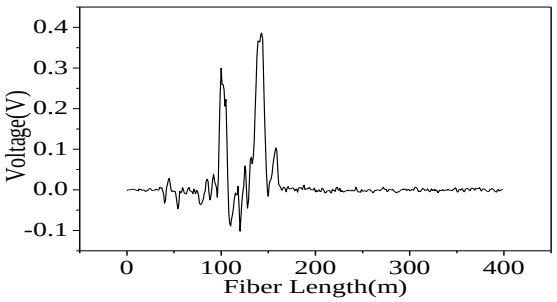

Figure 3.7: Simultaneous measurements of two pencil-break events

The SNR characters at different distances from the sensing fiber, different launched pulse power and different moving averaging time were also investigated and the experimental results are shown in Figure 3.8(a) and (b). Figure 3.8(a) shows the SNR changes with different moving averaging number at different input pulse peak power. As the pulse power increases to 28mW, a detectable signal at vibration point is obtained. For

the same pulse peak power, the SNR will firstly increase to a maximum value and then decrease. The optimum averaging number is around 200 due to the limited previous pencil-break event.

In Figure 3.8(b), the SNR decreases when the distance between the sensing fiber and the pencil-break event becomes larger under the same averaging time. The SNR under 4 moving averaging 18cm is smaller than 2, which means we cannot discriminate the signal from the noise floor due to high attenuation of the pencil-break generated pulse surface wave of aluminum plate.

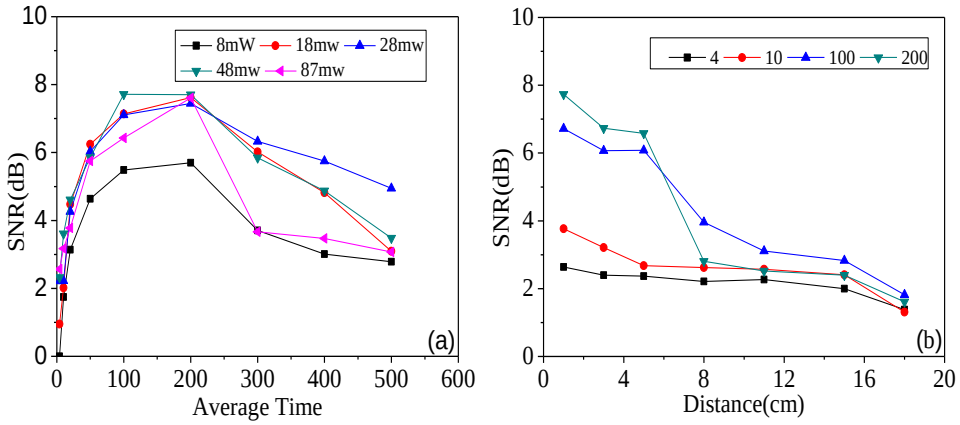

Figure 3.8: (a) relationship of SNR to moving average time at different input pulse power and (b) relationship of SNR to distance under different moving average time for injection pulse width 50ns.

3.4 Conclusions

We have described a phase-OTDR sensing system based on polarization-maintaining configurations for higher frequency response, distributed vibration measurement. The moving averaging time is reduced to 4 and the highest frequency response is improved to

2.25 kHz. The spatial resolution increases to 1m. A new layout of a straight line sensing fiber is adopted to replace the original fiber loops and the minimum interacting length of fiber and disturbance is decreased to 0.13m. The maximum distance between vibration event and the sensing fiber is 18cm with a SNR larger than 2 dB. This new phase-OTDR system is promising as a distributed vibration sensor for structural health monitoring.

Chapter 4

4 Wavelet denoising method for improving detection performance of phase OTDR system

We introduced a polarization-maintaining configuration to overcome the problem of signal fading and noise induced by the polarization states change in the single mode fiber in Chapter 3. Moving average and moving differential methods are used to reduce the noise floor in order to determine the location information of the vibration and the highest detectable frequency is around 2.25 kHz with the spatial resolution of 1m. However the system based on the all polarization-maintaining configuration is too complicated and expensive to be used for practical distributed sensing application.

The difficulty of vibration measurement, in comparison to the static measurement is that commonly used many trace averages is not usable due to the dynamic change of the signal, even with short interaction length and much weaker Rayleigh signal. Hence the signal processing scheme is critical in getting high performance distributed dynamic measurement. Although we have proposed the moving average and moving differential method to remove the noise and highlight the signals interested, this general filtering method is less effective with short pulse (<10ns) due to the broadband frequency and polarization induced noises in single mode fibers.

In this chapter, we introduce the wavelet denoising method [73, 74] to the phase-sensitive OTDR vibration sensor with coherent detection to eliminate the noise. Since wavelet transform has a built-in capacity of adapting to local changes along the fiber length, optimal denoised data could be obtained with an appropriate threshold algorithm to reject the random noises induced by varied polarization states in different position and detectors. Experimental results show a vibration event of PZT cylinder with a frequency as high as 8kHz with a 0.5m spatial resolution can be detected even in the single mode fiber.

4.1 Overview of wavelet denoising method

Wavelet analysis has become an emerging and promising tool with wide application such as data compression [75], signal and image processing [76, 77], pattern recognition[78] and so on in mathematics, physics, biology and engineering fields due to its distinguished advantages. Wavelet transform decomposes a signal into a series of base functions of dilated and translated versions of the mother wavelet function. The form of the continuous-time wavelet transform (CWT) of a signal $x(t)$ is defined as [79]:

$$X_{CWT}(a,b)=\frac{1}{\sqrt{a}}\int_{-\infty}^{\infty}\Psi^{*}(\frac{t-b}{a})x(t)dt \qquad a,b\in R\,\&\,a\neq 0 \tag{4.1}$$

Where a and b are the dilation and translation parameters, respectively. $\Psi^{*}(t)$ is the conjugate function of the mother wavelet.

Instead of continuously varying the parameters like the CWT which contains a large amount of redundant information we can analyze the signal with less number of scales

with varying number of translations at each scale, which is called the discrete-time wavelet transform (DWT) obtained by sampling the CWT with a dilation factor as powers of 2. The expression of the DWT is shown as below:

$$X_{DWT}(j,k) = \sum_{j,k} x_{j,k}(t) 2^{-j/2} \Psi(\frac{t-2^j k}{2^j}) \quad (4.2)$$

In this equation, j and k are dilation and translation factors. Mallat proposed a method using a bank of low-pass and high-pass quadrature mirror filters to compute the DWT [8]. Figure 4.1 shows the schemes of DWT and inverse DWT based on filter banks. The signal passes the filter banks and is decomposed into the approximation coefficients obtained from the low-pass filter and the detail (wavelet) coefficients obtained from the high-pass filter which are represented by $a_k^{(n)}$ and $d_k^{(n)}$, respectively. The decomposition levels and the filter coefficients are determined by the mother wavelet function. The mother wavelet function affects the shape of the signal at each level of decomposition. It is important to select an appropriate mother wavelet function according to the property of signals. Fig.1 shows that the low frequency component in the signal is analyzed by a narrow band filter at high decomposition level, while the high frequency component is analyzed by a broadband filter at the low decomposition level.

Wavelet shrinkage is a signal denoising method based on the idea of threshold wavelet coefficients of the noisy signal. Whereas the previous used moving average method [67, 80] removes high frequencies and retains low frequencies, the wavelet denoising method attempts to remove whatever noise is present and retain signal presented in the data

regardless the frequency content of the signal. The wavelet shrinkage method for phase OTDR system consists of three steps: 1) apply the DWT

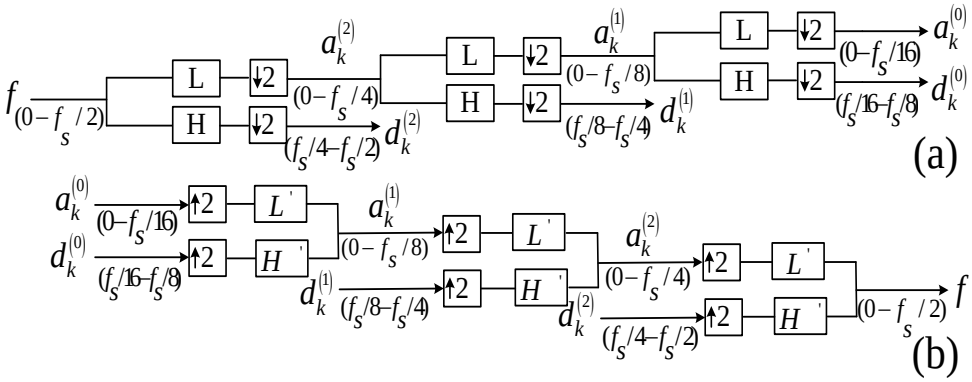

Figure 4.1: Schemes of DWT and Inverse DWT based on filter banks with decomposition level 3: (a) DWT, (b) Inverse DWT;L,L':low-pass filter; H,H': high-pass filter;fs:sample frequency

on the raw noisy backscattering Rayleigh traces to obtain the wavelet coefficients; 2) choose an appropriate threshold rule to the wavelet coefficients, and 3) reconstruct the denoised signal with the inverse DWT. Through the threshold step the wavelet coefficients of the noise can be eliminated since the noises embedded in the signal usually corresponds to the wavelet coefficients with small absolute value. The denoised traces are then being subtracted by their previous time trace at the same location to get position information of the vibration event. Then FFT is used for this event section to get the vibration frequency information.

4.2 Experimental setup

The experimental setup of the phase-sensitive OTDR with coherent detection is shown

in Figure 4.2. The light source is a narrow linewidth laser (NLL) (4 KHz) with highest power of 84mW. The continuous-wave (CW) light from the NLL is split by a 3dB coupler. An acoustic-optic modulator (AOM) is used to induce a 200MHz frequency shift to one output arm of the CW light from the coupler. Then the modulated light is amplified by the first Erbium-doped fiber amplifier (EDFA) (marked as 1st in Fig 2) to compensate a large insertion loss of the AOM. The output light is launched into an electro-optic modulator (EOM) to generate the pulses. The second EDFA (marked as 2nd in Fig 2) is used to amplify the pulses and the ASE noise is filtered by using an optical fiber Bragg grating. The amplified pulses are launched into a single mode sensing fiber by a circulator. Another arm of the coupler is used as a local oscillator which is combined with backscattered Rayleigh signals from fiber under test by a 3dB coupler. A balance detection scheme is used to eliminate the DC and common components and obtain 3dB SNR improvement.

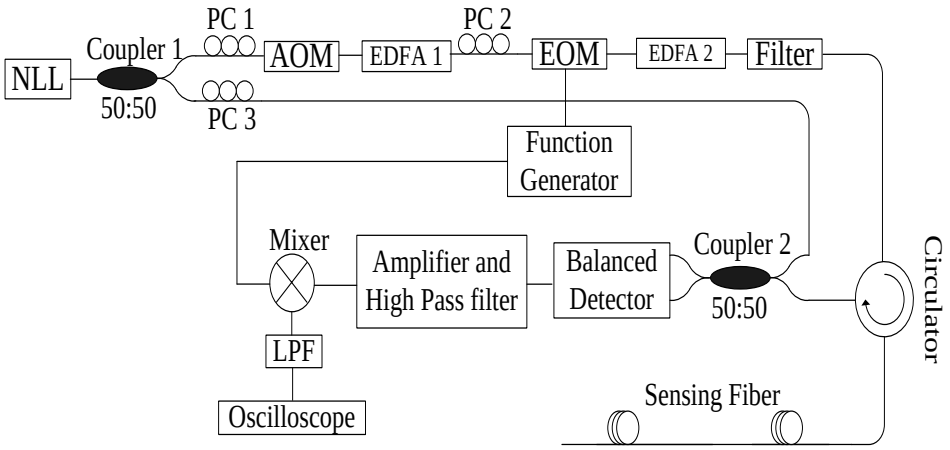

Figure 4.2: Experimental setup for coherent phase-sensitive OTDR, AOM: acoustic-optic modulator; EOM: electro-optic modulator; PC: polarization controller, Filter: optical fiber grating filter; LPF: low pass filter.

There are two main noises in the coherent heterodyne system: shot noise

$\sigma_s^2 = 2q(I + I_d)\Delta f$, here I_d is the dark current of detector, $I_d << I$, Δf is the bandwidth of receiver, and the thermal noise $\sigma_T^2 = (4k_B T / R_L)F_n \Delta f$, k_B is the Boltzmann constant, T is the absolute temperature, R_L is the load resistor, and F_n represents the factor by which thermal noise is enhanced by various resistors used in pre- and main-amplifiers. So the signal to noise ratio (SNR) can be expressed as following [32]:

$$SNR = \frac{\langle I_{ac}^2 \rangle}{\sigma^2} = \frac{2R^2 P_b P_{LO}}{2q(RP_{LO} + I_d)\Delta f} \tag{4.3}$$

The relationships between the SNR and pulse peak power under different pulse width and local oscillator power are investigated to find the optimized detection. Here the SNR has the same definition in Chapter 3 which is a voltage ratio between the mean voltage of the backscattered Rayleigh signal and the mean noise floor $SNR = 10\log(V_{Rayleigh} / V_{noise})$. In this experiment, the pulse repetition rate is 50 kHz because a high speed digital oscilloscope is used instead of DAQ-card and the pulse width is set at 20ns and 5ns respectively. 5000 backscattered traces are acquired for SNR calculation under different pulse peak power. Figure 4.3 shows the SNR evolution with the pulse peak power of 20ns and 5ns pulse width. It shows that the SNR increases almost linearly with the pulse peak power in both 20ns and 5ns case when the power of the local oscillator is -7.8dBm. This can be explained by that the system operates in the thermal noise limit regime due to low local power. Based on Eq. (4.3) SNR is proportional to the average signal power under thermal noise limit. When the local power increases to 0.2dBm the system changes to the shot noise limit regime and the thermal noise term can be neglected. The SNR increases with the pulse

peak power according to Eq. (4.3). However, Figure 4.3 shows that the SNR firstly increases to a maximum value and then decrease with the increase of the pulse peak power. The SNR degradation is caused by the gain saturation of the detection system, as our balance detector has high a gain of 10V/mW. Here the signal is saturated, but noise is kept, thus the SNR is reduced.

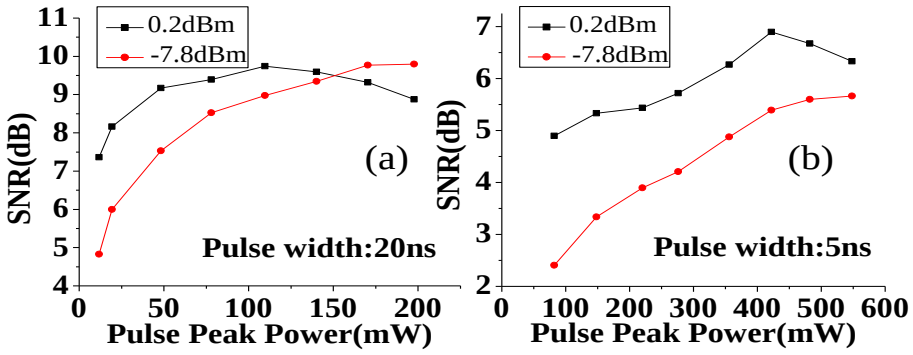

Figure 4.3: Signal to noise ratio changes with the pulse peak power under different pulse width and local oscillator power without vibration event: (a) 20ns pulse width, (b) 5ns pulse width

4.3 Experimental results of PZT vibration

4.3.1 Comparison between two denoising methods

The denoising capability of moving average method and wavelet denoising method are compared and analyzed firstly using the raw traces of the pencil-break event discussed in previous chapter. Figure 4.4 shows the denoised Rayleigh backscattering time-domain traces by using moving average method with 100 time average and wavelet denoising method, respectively. We can find that the amplitude fluctuations among traces are still

obvious at the fiber regions without pencil-break event due to the residual noise after moving average process. In contrast, Figure 4.4(b) represents the denoising traces after wavelet denoising method. Noise-free traces can be obtained and the unique feature of the coherent Rayleigh backscattering light in time-domain can be completely retrieved. Moving average method can be regarded as a low-pass filter which can only remove the noise in the high frequency region. The amplitude variation in Figure 4.4(a) is mainly caused by the residual low frequency noise. Wavelet denoising method assumes that the coefficients corresponding to the signal parts are much larger than those corresponding to the noise parts distributed in the entire bandwidth. After performing the DWT, a threshold value is set to eliminate the coefficients of the noise and keep the component of the signal. Therefore both the noise in low and high frequency regions can be removed and a much more "clean" denoising trace can be obtained.

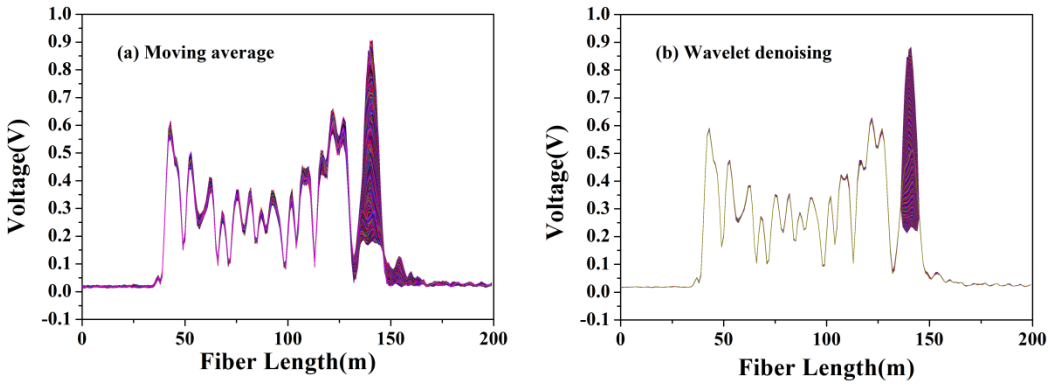

Figure 4.4: Denoised Rayleigh backscattering time-domain traces of pencil-break event using (a) moving average method and (b) wavelet denoising method.

Figure 4.5 shows the position information for the pencil-break event using moving average method and wavelet denoising method, respectively. The height of the peaks representing the position of the pencil-break event is almost the same in both methods. However the noise floor of the moving average method is much higher than the wavelet denoising method.

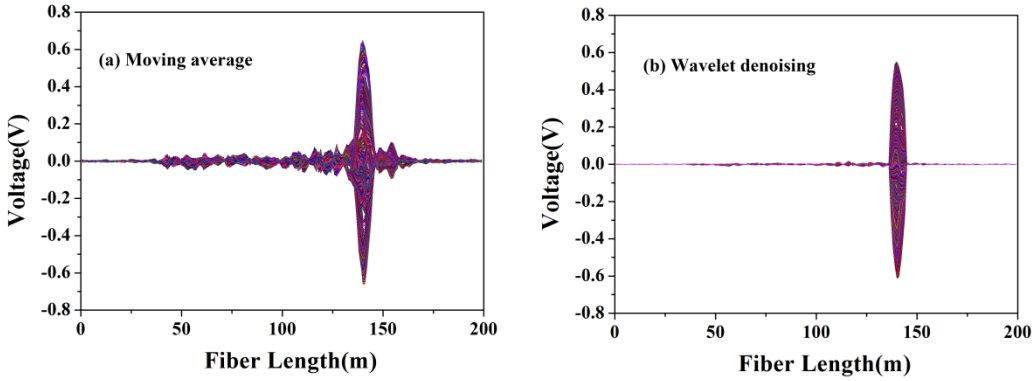

Figure 4.5: Traces of position information for the pencil-break event using (a) moving average method and (b) wavelet denoising method.

4.3.2 Detection of PZT vibration

A PZT cylinder with 0.6m single mode fiber wound is put into the fiber under test around 545m of 1km sensing fiber in our system as a vibration source as shown in Figure 4.6. The PZT is driven by a function generator and the frequency can be adjusted from several Hz up to kHz. The fiber is fixed on the surface of the PZT cylinder by instant glue and the vibration of the PZT can be transmitted to the fiber.

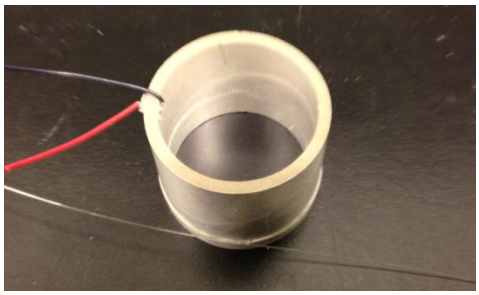

Figure 4.6: PZT cylinder used as a vibration source with 0.6m single mode fiber on it

In our experiment, the pulse width is 5ns and the pulse peak power is round 420mW which can give a best SNR under 0.2dBm local oscillator power. 1000 traces were recorded by an oscilloscope with 500MHz sampling rate. Each data point represents 0.2m along the sensing fiber. Considering the different frequency range of the vibration event, the pulse repetition rate varies from 10 kHz to 50 kHz. Figure 4.7 (a) and (b) show the position information of the vibration source of 20Hz and 8 kHz, respectively. The noise level of the 20Hz is lower than the 8 kHz. The reason is that the wavelet coefficients of the noise at high frequency are kept after wavelet denoising due to the broad bandwidth of the filter for high frequency signal. Since the vibration signal from the PZT is stationary, the frequency can be obtained by applying Fourier transform on the raw traces. Figure 4.7(c) and (d) are the power spectrums of 20Hz and 8 kHz vibration events.

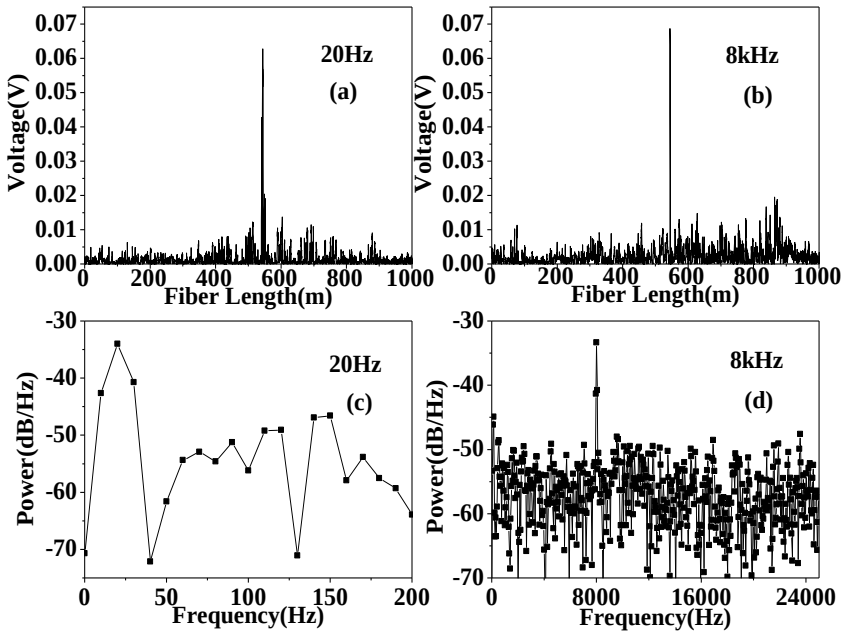

Figure 4.7: PZT vibration detection with 5 ns pulse: (a) position information of 20Hz vibration event, (b) position information of 8kHz vibration event, (c)power spectrum of 20Hz vibration event, (d)power spectrum of 8kHz vibration event

4.4 Conclusions

The application of wavelet denoising method to the distributed vibration sensing in phase-sensitive OTDR system is described in this chapter. The disturbance induced signal change can be exacted from the excessive noise background effectively by wavelet denoising method compared to the moving averaging method which proved to be a powerful tool to enhance the performance of phase OTDR system. The denoising performance for the moving average method and wavelet denoising method has been compared by using the pencil-break event. A vibration event up to 20 kHz using PZT cylinder is measured with a spatial resolution of 0.5m.

Chapter 5

5 Time-division multiplexing phase OTDR for distributed vibration sensing

This chapter discusses a new scheme for the measurement of vibration event with high frequency in phase-sensitive OTDR system. Section 5.1 shows the motivation of this new technique. The principle of this novel time-division multiplexing scheme and the experimental setup are introduced in Section 5.2. Section 5.3 presents the experimental results of position and frequency information for a PZT vibration event.

5.1 Introduction

In the prior two chapters, the detection performance of the distributed vibration sensor based on phase-sensitive OTDR has been improved by both hardware and software methods. However, as mentioned before for the applications of vibration sensors in health monitoring and damage detection of civil infrastructures and mechanical processes, frequency information of these vibration events is usually from sub-ten Hz to hundreds of kHz. In order to extract the accurate frequency information as well as the location information, a distributed optical fiber vibration sensor with high frequency response and high spatial resolution is truly desirable. Usually, both the position and frequency

information of the vibration event are accessed simultaneously in the phase-sensitive OTDR system described before. The position information is determined by compared the differences among the Rayleigh backscattering traces and the frequency information is obtained by the power spectrum through FFT of the time trace picked up from the raw Rayleigh traces at the vibration point. In order to perfectly retrieve the frequency information of the vibration event the pulse repetition rate f_r has to meet the criterion $f_r > 2f_v$ according to the Nyquist sampling theorem where f_v is the highest frequency components of the interested vibration event. In real measurement this criterion is much stricter which requires $f_r > 5f_v$ avoiding signal distortion. The fundamental obstacle which limits the accessible frequency response in phase-sensitive OTDR system is that the pulse repetition rate cannot increase without limitation. The sensing fiber length will be shortened as the increment of pulse repetition rate. For example the allowed fiber length is only 40 meters when the pulse repetition rate is set to be 2.5MHz. In this chapter, we proposed a novel time-division multiplexing (TDM) scheme based on the phase OTDR system to achieve distributed vibration sensing with high frequency response and high spatial resolution. By designing the time-domain shape of the probe waveform, the phase OTDR system and the polarization diversity setup can be combined together in the same sensing fiber region at different time slots. Experimental results show that PZT vibration events from 1Hz to 0.6MHz can be measured with 1m spatial resolution along 680m single-mode sensing fiber.

5.2 Principle and Experimental Setup

Figure 5.1 describes the temporal evolution of the probe waveform used in the TDM phase OTDR. The whole waveform consists of one narrow pulse with width and one quasi continuous wave (CW) offset with duration time which is followed by two idle time section separately. This well-designed waveform can guarantee that two measurement systems including phase OTDR for position detection and polarization diversity setup for frequency detection of the vibration event, can be merged in one single-mode sensing fiber without crosstalk. The probe light is launched into the sensing fiber from one end and the amplitude changes induced by the vibration could be obtained by the narrow pulse with high power. At the output end, the frequency information of the vibration can be retrieved with the small quasi-CW light using the polarization diversity setup by monitoring the power variations of the transmitted light due to the polarization state changes induced by the vibration. In order to avoid the deterioration of the SNR and perform unambiguous detection for position information of the vibration caused by the Rayleigh backscattering noise from the quasi-CW light, two idle time sections, which are longer than the round-trip time, are located between the pulse and the quasi-CW light.

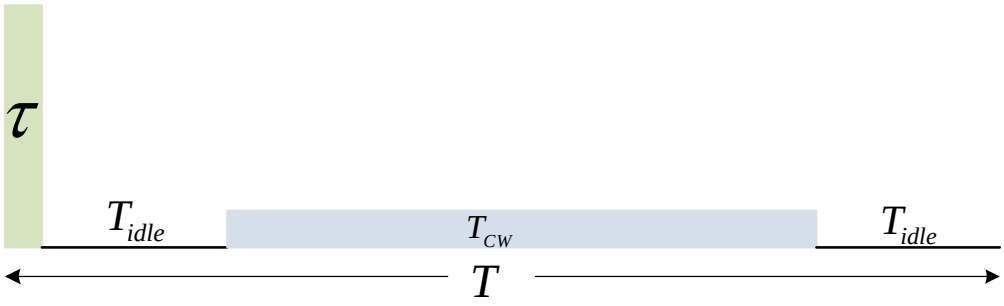

Figure 5.1: Lightwave shape for time-division multiplexing phase OTDR. (T: pulse period ,τ: pulse width, T_R: round-trip time and T_{CW}: time of the small quasi continuous wave (CW) light)

The position information of high frequency vibration event can be determined using the phase OTDR part in the new system with a pulse repetition rate which is much lower than the signal frequency. Commonly the sampling frequency must be greater than or equal to twice the highest frequency component in the interested signal in order to reconstruct the signal perfectly without any losses of information. However we only care about the relative amplitude difference among Rayleigh traces induced by the external disturbance instead of absolute value for the application of vibration sensing. The position information can be obtained by comparing the relative amplitude variations. Figure 5.2 provides a simple example to illuminate the signal distortion caused by undersampling. Black curve in Figure 5.2 represents a 95Hz sinusoid waveform with an arbitrary initial phase. This signal is acquired by three different undersampling rates. Results show that none of the sampling rates can rebuild the original signal due to the violation of Nyquist sampling theorem. Especially when the signal frequency is the integer multiple of the sampling rate the acquired signal is a DC signal with amplitude determined by the initial phase, as shown by the red curve in Figure 5.2 Except this special case, the amplitude of the distorted signal still varies with

time as long as the amplitude of the original signal is time-dependent.

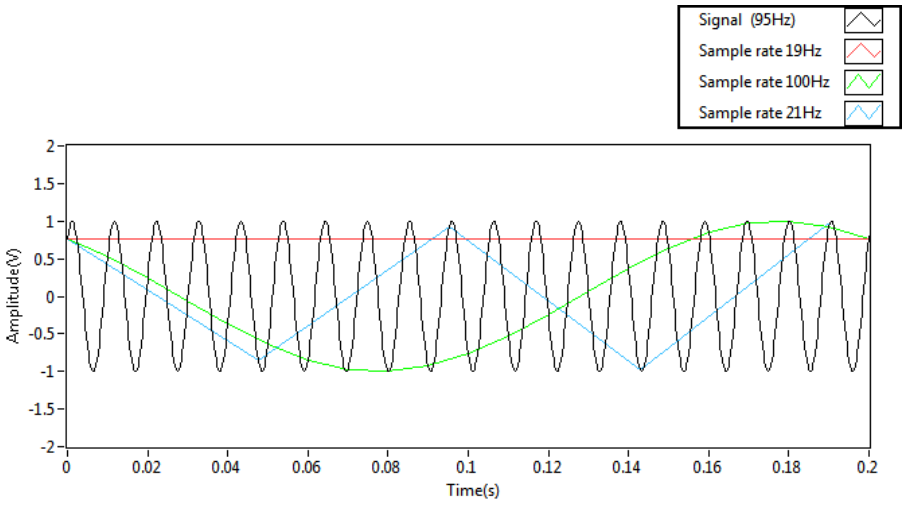

Figure 5.2: Shapes of a sinusoid signal of 95Hz at different undersampling rate.

The frequency information of the vibration event is detected by using the polarization diversity scheme implemented by PBS in conjunction with a balanced detector. Figure 5.3 shows a simple sketch of vibration sensing based on polarization diversity scheme. The CW light from a laser source is launched into the sensing fiber. The state of polarization (SOP) of the input light is adjusted by a polarization controller in order to balance the power of the two outputs of the polarization beam splitter at the output end of the sensing. The sensitivity is optimized to be the largest when the light is launched into the fiber with an angle equal to $\pi/4$ between the polarization plane and the fast axis of the PBS [81].

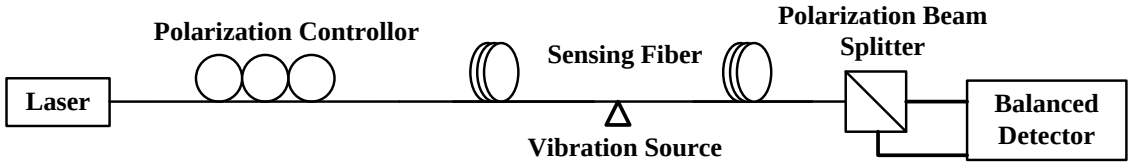

Figure 5.3: Sketch of the vibration sensing setup based on polarization diversity detection using the transmitted light.

Considering an external vibration source located at certain position along the sensing fiber, the SOP of the output light will be rotated with a small angle θ induced by the vibration. The output signal from the balanced detector can be expressed as:

$$\begin{aligned} I &= \eta \cdot P_0 \left[\cos^2\left(\frac{\pi}{4}+\theta\right) - \sin^2\left(\frac{\pi}{4}+\theta\right) \right] \\ &= -\eta \cdot P_0 \sin 2\theta \approx -2\eta \cdot P_0 \theta \end{aligned} \tag{5.1}$$

where η is the optical-electrical conversion coefficient and P_0 is the incident light power of the PBS.

If only one of the outputs of the PBS is detected, the signal is given by:

$$\begin{aligned} I_s &= \eta \cdot P_0 \cos^2\left(\frac{\pi}{4}+\theta\right) = \frac{1}{2}\eta \cdot P_0 (1-\sin 2\theta) \\ &\approx -\eta \cdot P_0 \theta + \frac{\eta \cdot P_0}{2} \end{aligned} \tag{5.2}$$

The condition for validating the approximations in the above equations is that the SOP rotation angel θ is small enough. We can easily find that the polarization detection scheme offers two benefits over the single-channel detection: the DC portion is removed and the SNR is enhanced by 3dB. By observing the output power variation caused by the SOP change, the frequency information of the vibration can be determined.

Figure 5.4 is the experimental configuration of the TDM phase-sensitive OTDR. The light

from a narrow linewidth laser (NLL) is splitter into two parts by a 3dB optical coupler. The probe waveform for TDM phase OTDR is programed by an arbitrary function generator which drives an electro-optic modulator (EOM) to generate the optical signal. Before launching into the sensing fiber through a circulator, the light wave is firstly amplified by an Erbium-doped fiber amplifier (EDFA) and then filtered by an optical fiber grating filter to remove the ASE noise. For phase-OTDR system, the Rayleigh backscattering signals generated by the narrow pulse are combined with the local oscillator light with a 200 MHz frequency shift induce by an acoustic-optic modulator and then collected by a balanced-detector. For the polarization diversity scheme, a polarization beam splitter (PBS) is positioned to separate the transmitted light into two orthogonally polarized lights, which are also detected by a balanced-detector. There will be a relative π phase shift between the two outputs of the PBS when it is balanced by the polarization controller (PC) at the input end of the sensor fiber [81]. The vibration source is a PZT cylinder with 3cm diameter. 6 loops of fiber corresponding to around 60cm long are glued on the surface of the PZT tube. The PZT tube works under a driving signal from a function generator. In our former experimental setup [80], an electrical mixer is used to convert the intermediate frequency (IF) signal to the baseband. However this synchronous demodulation scheme is sensitive to the variation of the intermediate frequency, and typically a frequency locked loop is needed. The frequency drift of the AOM during measurement makes the SNR of the detection system fluctuate. Here we simplify our setup by removing the demodulation scheme. Due to the interference effect of the backscattering Rayleigh light wave within the pulse width, both the amplitude and phase of the signals have been encoded by the external vibration information before being combined with

the local oscillator light so that the vibration event can be determined without recovering the baseband signals.

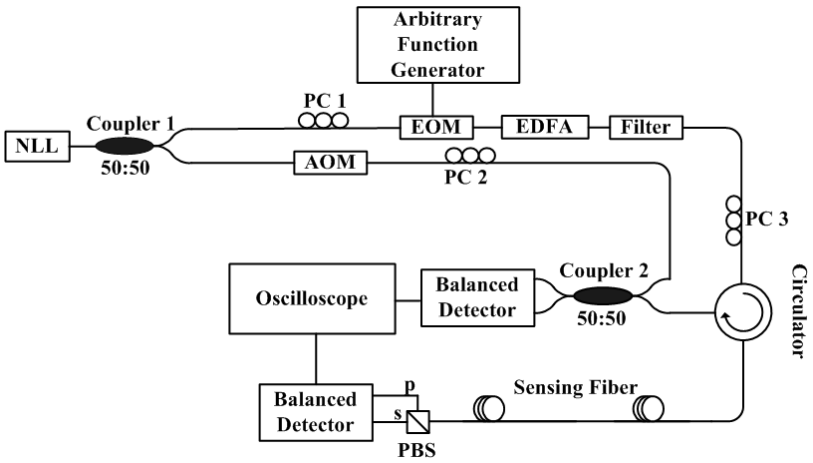

Figure 5.4: Experimental configuration of TDM phase OTDR. NLL: narrow linewidth laser; AOM: acoustic-optic modulator; EOM: electro-optic modulator; EDFA: Erbium-doped fiber amplifier; PC: polarization controller, Filter: optical fiber grating filter, PBS: polarization beam splitter.

5.3 Experimental results and discussions

5.3.1 Detection of high frequency vibration events

We firstly test the detection capability for high frequency vibration event of the TDM phase OTDR system. The repetition rate of the probe waveform is 2.0 kHz which is corresponding to a period T 500μs. A narrow pulse of τ=10ns is used and the duration time for the quasi-CW light T_{CW} is equal to 400μs. The idle time section T_{idle} is 50μs which is much larger than the round-trip time of the 680m sensing fiber. The noise floor of the Rayleigh backscattering signals from the pulses is not affected by the Rayleigh backscattering light from the quasi-CW offset due to the idle

time. The PZT cylinder is under the vibration driven by a 0.6MHz sinusoid waveform from the function generator. Although the frequency of vibration event is an integer multiple of the pulse repetition rate, the real frequency is not exact 0.6MHz due to the limitation of the frequency accuracy of the function generator. The frequency accuracy is 0.01% which means a fluctuation around ± 60 Hz of the signal frequency. Therefore the amplitude variation of the Rayleigh backscattering traces induced by the vibration can still be detected. Figure 5.5 shows the superposition of 200 Rayleigh backscattering traces after wavelet denoising signal processing method discussed in Chapter 4. We can find an obvious amplitude changes (circled in red dashed line) among the different traces at the position under the vibration because the amplitude information at discontinuous periods of the fast vibration signal could be acquired by the probe narrow pulse with a slower rate. However the unambiguous frequency information cannot be recovered due to the requirement of Nyquist sampling theorem. At other positions along the sensing fiber without vibration, the amplitudes keep almost the same for the 200 traces.

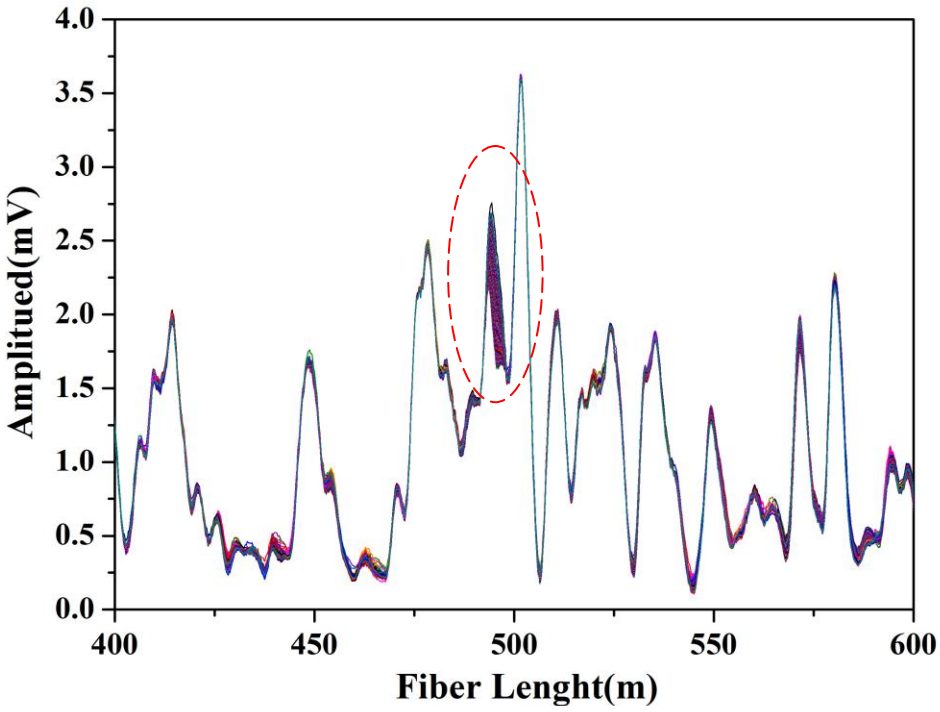

Figure 5.5: 200 raw Rayleigh backscattering traces after wavelet denoising signal processing method for 0.6 MHz PZT vibration event.

Therefore the position information of the vibration which is shown in Figure 5.6 can be obtained by successive subtraction among the traces. A significant peak represented the position of the vibration event is located around 500m along the fiber.

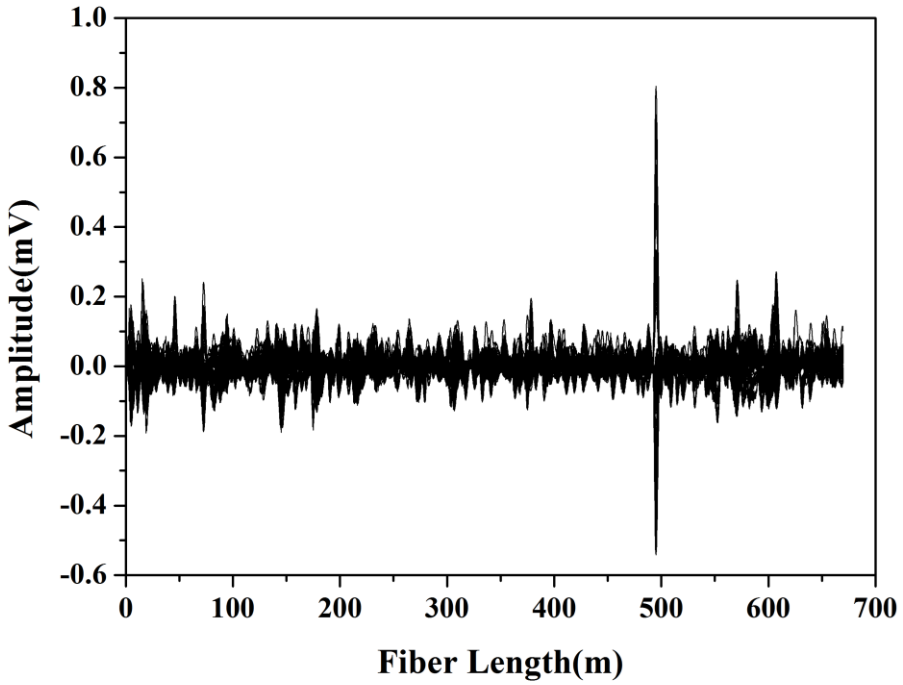

Figure 5.6: Position information of the 0.6 MHz PZT vibration event with 10ns pulse width

Frequency information of the vibration event is obtained from the transmitted quasi-CW light using the polarization diversity detection scheme. The sampling frequency of the digital oscilloscope is 100Mhz. Considering the during time 400μs of the quasi-CW light, the total number of data points is 40000 and the frequency resolution is 2kHz which is good enough for the frequency measurement on the order of several hundreds of kHz. A small DC bias is applied on the EOM to generate the quasi-CW light. The value of this DC bias needs to be chosen carefully. The optical gain of the pulse amplified by the EDFA will be influenced if the quasi-CW light is too strong because the pump power is depleted by the quasi-CW part. The signal can also be immerged in the large floor of the residual ASE noise when the DC bias is too small. In our experiment, the DC bias is set to be 200mV corresponding to an optical power around -18.3dBm. Figure 5.7 (a)

shows the time-domain signals of the 0.6 MHz PZT vibration event. Black curve represents the original signals acquired directed from the detector which looks quite noisy due to the ASE noise. However, we can still observe the sinusoid profile of the signal evidently. A clear sinusoid waveform can be obtained by using a digital band pass filter with bandwidth of 100 kHz and central frequency 0.6 MHz, which is shown as the red curve in Figure 5.7 (a). The power spectrum of the 0.6MHz vibration event is presented in Figure 5.7 (b). The raw signal without any digital filter is used to perform the FFT step. The amplitude of the signal peak is almost 40dB higher than the noise floor in frequency domain even the SNR in time domain which is shown in Figure 5.7 is very poor. There is no any higher order harmonic peaks existing in the power spectrum proved that the polarization diversity detection for frequency measurement has a very good linearity.

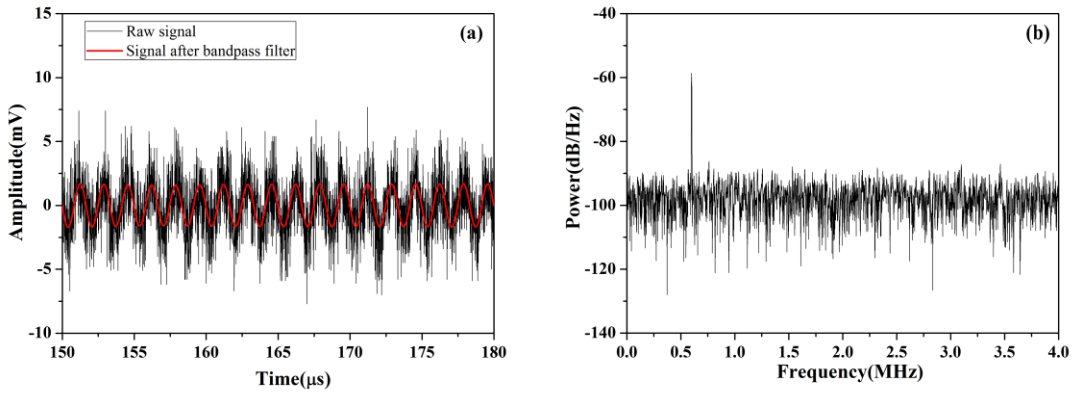

Figure 5.7: a. Time-domain signal of 0.6MHz vibration event, b. power spectrum of 0.6MHz vibration event.

5.3.2 Detection of low frequency vibration events

Besides the detection capability for the vibration with very high frequency, vibration event with frequency on the order of Hz can also be measured by analyzing the Rayleigh backscattering traces

obtained by the phase-sensitive OTDR system. In order to interrogate the low frequency region, the pulse repetition rate is set to be 5 kHz which means that higher frequency noise can be blocked directly by the system bandwidth. Total 10000 traces are acquired for a frequency resolution of 0.5Hz. Figure 5.8 presents the position and frequency information of 1Hz PZT vibration event. The position of the vibration is determined by comparing the Rayleigh backscattering traces after wavelet denoising and the frequency is obtained by applying FFT on the points under vibration. According to the above discussion, the presented time-division distributed vibration sensor could measure the vibration events with a broad band from 1Hz up to 0.6 MHz by adjusting the pulse repetition rates.

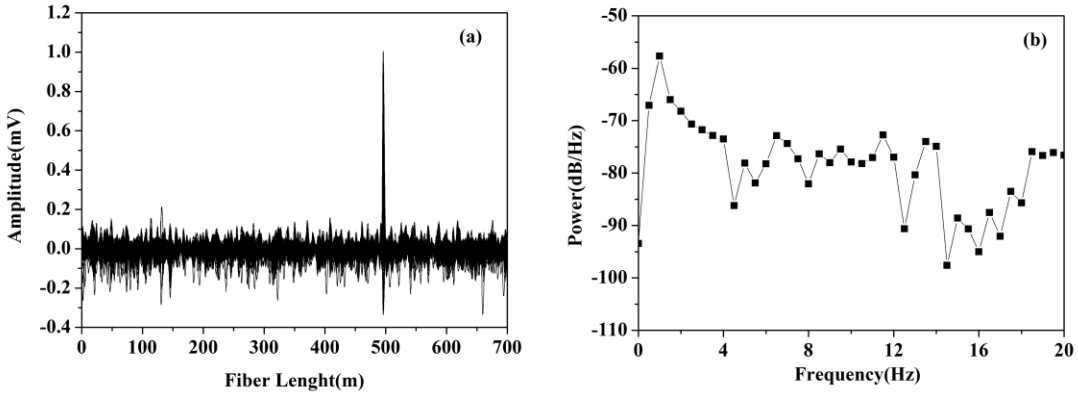

Figure 5.8: PZT vibration detection of 1Hz with 10 ns pulse: (a) position information of 1 Hz vibration event (b) power spectrum of 1Hz vibration event.

5.4 Conclusions

In this chapter, a new distributed vibration fiber sensor combined the phase-sensitive OTDR system and polarization diversity detection together is discussed for measurement

of high frequency vibration event. The two systems work in sequence through the time division multiplexing technique accomplished by a well-designed probe waveform. Although the frequency of the interested vibration event is much higher than the pulse repetition rate of the phase-sensitive OTDR, which means the original signals are distorted due to the undersampling rate, the position information can still be obtained since the amplitude changes at the fiber region under vibration occurred in different periods of the vibration signal are acquired. The frequency information is determined using the polarization diversity detection scheme by measuring the power change caused by the SOP change. A vibration event with 0.6 MHz frequency is tested. Both the position and frequency singles have a very good SNR. The maximum accessible frequency for the present system is only limited by our PZT cylinder which can only provide a frequency up to 0.6MHz.

Chapter 6

6 Continuous wavelet transform for non-stationary vibration detection with phase-OTDR

6.1 Introduction

Fully distributed capability of optical fiber sensor makes it a powerful tool to measure the environment changes along the sensing fiber. For health monitoring on civil structures and fault diagnostics of mechanical structures, optical fiber vibration sensors can be used to evaluate structural condition and identify internal damages at early stage through measuring the intrinsic frequency. Different schemes have been proposed to fulfill the distributed vibration sensing, such as using the polarization optical time-domain reflectometry (OTDR) [30, 49], Sagnac or Mach-Zehnder interferometers [17, 82]. In the aforementioned methods, vibration events are usually under the stationary conditions so that the vibration frequency analysis has generally relied on the spectral analysis via fast Fourier transform (FFT). An important limitation of the FFT is its inability to provide the time dependence of the signal spectrum. In practice, the interested realistic signals such as the cracks and fatigues inside the structures are usually transient and non-stationary which means that the conventional FFT approach is not able to reveal the inherent feature within the signals. Consequently, supplementary signal processing scheme of non-stationary

signals is critical for health monitoring and fault diagnostics based on fiber vibration sensing.

Time-frequency signal analysis methods can interpret signals in both time and frequency domain simultaneously compared to the commonly-used FFT. A number of time-frequency analysis techniques are available to decompose complex signals in time–frequency domain, including short time Fourier transform (STFT), Wigner-Ville transform (WVT), and continuous wavelet transform (CWT). These methods map the signal under investigation into a two dimensional (2D) function of time and frequency and therefore can provide true time-frequency representations. However the time and frequency resolutions of the STFT cannot be improved simultaneously because of the fixed time-bandwidth product for a defined window function. The WVT will generate the interference terms and tend to mislead the signal analysis. In comparison, the CWT has developed as the most favored tool [83, 84] because of its ability to decompose the signal by employing a window of variable width compared to other methods. Another key advantage of the wavelet technique is the variety of wavelet functions available to capture the subtle changes of the signal under investigation.

In this chapter, we introduce the CWT method to the phase-sensitive OTDR vibration sensor with coherent detection to analyze the non-stationary vibration signals [85]. Experimental results show a sweep vibration event with a frequency range of 500Hz to 1kHz can be detected along a single mode sensing fiber over 20cm disturbance length. The time dependent frequency information of the vibration event is determined from the CWT scalogram by wavelet ridge detection. The vibration position information is obtained by the wavelet global spectrum. This CWT method shows the potential of interrogating the

complex non-stationary vibration signals for damage detection in civil and mechanical related applications with the phase sensitive OTDR.

6.2 Continuous wavelet transform

Wavelet transform decomposes a signal into a series of base functions of dilated and translated versions of the mother wavelet function. The form of the continuous wavelet transform of a signal is defined as [79]:

$$W_f(u,s) = \int_{-\infty}^{\infty} f(t) \frac{1}{\sqrt{s}} \psi^*(\frac{t-u}{s}) dt \tag{6.1}$$

where $f(t)$ is the original signal, s and u are the dilation and translation parameters, respectively. $\psi^*(t)$ is the conjugate function of the mother wavelet. The CWT can measure the time evolution of frequency transients by using a complex analytic wavelet which can separate the amplitude and phase information of the signals. To be classified as a complex analytic wavelet, the wavelet function must meet the mathematical criteria that the Fourier transform of it should vanish for negative frequencies. Square of modulus of the CWT is known as the scalogram and is defined as:

$$E(u,s) = \left| W_f(u,s) \right|^2 \tag{6.2}$$

In Eq. (6.1), the spectral components of the signal are inversely proportional to the wavelet scale s and the location u represents the time information. Considering f_c is the characteristic frequency of the mother wavelet function, the frequency corresponding to a certain wavelet at an arbitrary scale is defined as:

$$f = \frac{f_c}{s} \tag{6.3}$$

The time-frequency resolution of the complex analytic wavelet depends on the time-frequency spread of the wavelet $\psi_{u,s}$ which corresponds to a Heisenberg box centered at (u,s) in the time-frequency plane. The area of this box remains constant at all scales but the resolution in time and frequency depends on the scale s . Hence the frequency accuracy will be affected when the CWT is used to analyze the vibration signal in phase-OTDR system. In general, the instantaneous frequency could be extracted by wavelet ridge detection in the time-frequency analysis using CWT method which could further alleviate the impact of noises on the signal interested. The wavelet ridge is defined by:

$$\frac{d(\left|W_f(u,s)\right|^2 / s)}{ds} = 0 \tag{6.4}$$

which corresponding to the local maxima at a specific scale s .

If the integral taken over all the time sections at a specific scale s , a global wavelet power spectrum similar to the classical power spectrum via FFT method could be obtained which is shown in Eq.(6.5):

$$E(s) = \int_{-\infty}^{\infty} \left|W_f(u,s)\right|^2 du \tag{6.5}$$

The peaks in this global power spectrum represent the dominant frequency components in the signal under investigation.

6.3 Experimental setup and signal processing

Compared with the conventional OTDR, the phase-sensitive OTDR utilizes a laser source with narrow linewidth and low frequency shift to form the interference of the backscattered light waves. The Rayleigh backscattering trace returned from the test fiber is modulated in the form of speckle-like profile [42] because of the coherent interaction of multiple scattering centers within the injected pulse duration. If there is no vibration along the sensing fiber, the amplitude of all the Rayleigh backscattering traces will be constant. When the vibration is applied on the certain section of the fiber, the amplitude of the Rayleigh backscattering light will be modulated and change in different time traces.

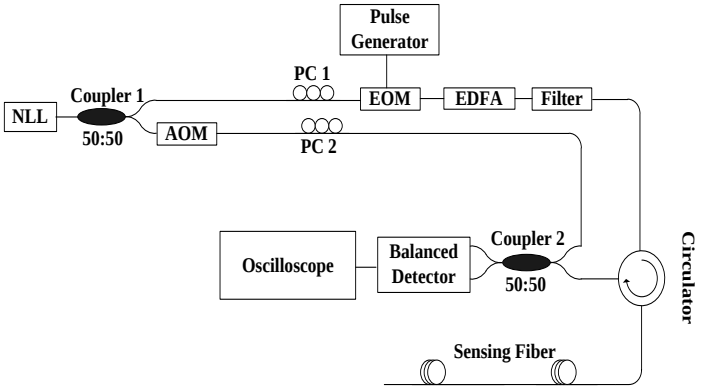

Figure 6.1: Experimental setup for coherent phase-sensitive OTDR, NLL: narrow linewidth laser; AOM: acoustic-optic modulator; EOM: electro-optic modulator; EDFA: Erbium-doped fiber amplifier; PC: polarization controller, Filter: optical fiber grating filter.

The experimental setup of the phase-sensitive OTDR with coherent detection is shown in Figure 6.1. The light source is a narrow linewidth laser (TeraXion) with maximum output power of 30mW and linewidth of 535 kHz. The continuous-wave (CW) light from the laser is split by a 3dB coupler. One output arm of the CW light from the coupler is injected into an electro-optic modulator (EOM) to generate the pulses. An Erbium-doped

fiber amplifier (EDFA) is used to amplify the pulses and the ASE noise is filtered by an optical fiber Bragg grating. The amplified pulses are launched into a single mode sensing fiber by a circulator. Another arm of the coupler is used as a local oscillator with a 200MHz frequency shift induced by an acoustic-optic modulator (AOM). Then the light of the local oscillator is combined with the backscattered Rayleigh signals returned from the fiber under test by a 3dB coupler. A balance detection scheme is used to eliminate the DC and common components and obtain 3dB signal-to-noise-ratio (SNR) improvement. The final signals are acquired by a high-speed oscilloscope and then the signal processing scheme is accomplished by a software program.

In order to reduce the amplitude fluctuation in the Rayleigh signal traces due to phase noise of the laser, partial interferometric problem (random polarization), and electrical noises such as thermal noise and shot noise, the wavelet denoising method [86] is introduced to enhance the interested signals. This signal denoising method is based on the idea of threshold wavelet coefficients of the noisy signal using the discrete wavelet transform to remove the noise. Hundreds of the Rayleigh backscattering traces from the sensing fiber are collected and then pass a digital low pass filter to remove firstly the high frequency noise. The points on each curve represent the positions along the fiber. The signals at a certain position of all the traces will be extracted and plotted versus time to form a new time domain sequence. After wavelet denoising on these new sequences, the CWT method will be applied to find the time-evolved frequency information. In order to determine the position of the vibration event, the global wavelet power spectrum at each position is calculated and a 2-D graph with fiber length and frequency information can be drawn to show the location of the vibration.

6.4 Experimental results and discussions

A PZT cylinder with 0.2m single mode fiber wound is put at 72.3m over 200m sensing fiber in our system as a vibration source. The PZT is driven by a function generator and the frequency can be adjusted from several Hz up to kHz. The fiber is fixed on the surface of the PZT cylinder by instant glue and the vibration of the PZT can be transmitted to the fiber. In our experiment, the pulse width is 10ns and 1000 traces are recorded by a high-speed oscilloscope with 1GHz sampling rate. The pulse repetition rate is fixed at 10 kHz and total data acquisition time is 0.1s. The maximum sensing length of the phase OTDR system is related to the repetition rate of the pulse. The time interval among the pulses should be larger than the round trip time that the pulses travel in the sensing fiber to keep only one pulse inside the sensing fiber. For the 10 kHz repetition rate, the detection range is around 10km which is determined by $L < (c/2nf)$, where L is the sensing fiber length, c the speed of light, n the group index of the fiber and f the repetition rate of the pulse. The sensing length can be extended by launching pulses with a higher peak power. A stationary vibration event with the frequency 500Hz is tested firstly. The position is determined by the amplitude difference among the global wavelet spectrum of different time sequences. Compared to the small amplitudes of the global wavelet spectrum at the fiber sections without vibration, there will be some peaks corresponding to the frequency of vibration at the location under the disturbance. Figure 6.2 shows the contour plot of the global wavelet power spectrum along the fiber length for the stationary vibration detection

of 500Hz using the digital low pass filter with different cutoff frequency.

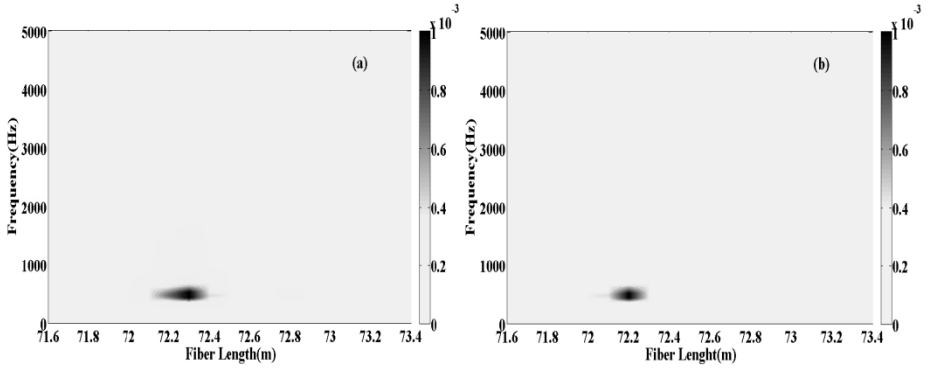

Figure 6.2: Contour plot of the global wavelet power spectrum along the fiber length for the stationary vibration detection of 500Hz (a) 200MHz low pass filter (b) 350MHz low pass filter.

Since the signal with the vibration information is in the IF range around 200MHz and the bandwidth of the detector is 350MHz the high frequency electrical noise should be removed in order to obtain a better SNR. As shown in Figure 6.2, two low pass filters with cutoff frequency 200MHz and 350MHz are tested separately. We find that the SNR can be optimized by a digital low pass filter with 200MHz cutoff frequency compared to 350MHz which can remove the high frequency electrical noise above the IF frequency and retain the useful information simultaneously. Here the SNR of the location information is defined as an amplitude ratio between the signal peak amplitude and the background noise level SNR=10*log (A_{signal}/A_{noise}). According to this definition, the SNR of the 200MHz cutoff frequency filter is 20.7dB compared to the 350MHz case which is 18.1dB. The global wavelet transform spectrum at each point along the sensing fiber is obtained to determine

the position by integral over the whole data acquisition time which can amplify the signal section and suppress the noise level.

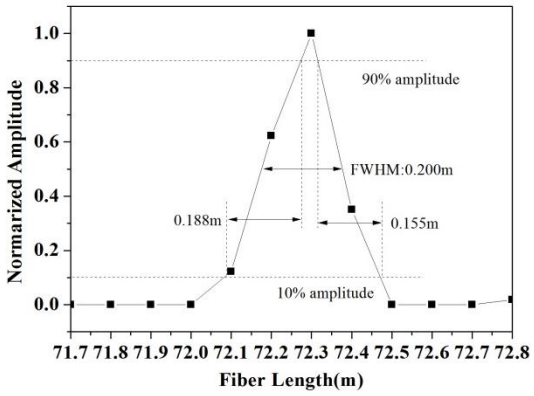

Figure 6.3: Position profile of the 500Hz vibration event with 10ns pulse width using the 200MHz low pass filter.

The position profile of the 500Hz vibration event with 10ns pulse width using the 200MHz low pass filter is shown in Figure 6.3. Here the spatial resolution is defined by the average of the rise and fall time equivalent fiber length for the small section under the disturbance [87]，then spatial resolution around 0.172m is achieved. The 20cm fiber section under vibration is also clearly identified by the full width half maximum (FWHM) in Figure 6.3.

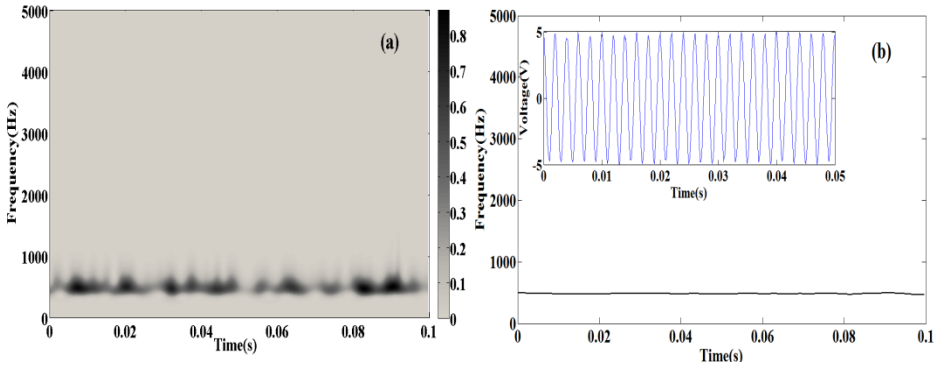

Figure 6.4: (a) Scalogram of the 500Hz stationary vibration event at the vibration position (b) instantaneous frequency obtained by wavelet ridge detection.

Figure 6.4(a) is the scalogram of the 500Hz stationary vibration event at the vibration position. It shows the frequency evolution with time of the vibration event which keeps constant in this case during the data acquisition process. The scale value is 256 which mean there are 256 points corresponding to the half sample frequency after CWT. The frequency accuracy is about 5000Hz/256=19.5Hz. The amplitude of the scalogram at around 500Hz changes along the time because the amplitude fluctuation of the time-domain traces induced by the noises. From Figure 6.4(a), we can also find a frequency spreading which is determined by the time-frequency resolution of the CWT method. The frequency spreading will cause the accuracy of frequency measurement to decrease. This problem could be solved by the wavelet ridge detection method which can determine the instantaneous frequency. The instantaneous frequency in Figure 6.4(b) is extracted from the scalogram by wavelet ridge detection method. It provides more accurate frequency information for the further analysis in real applications. The inset graph in Figure 6.4(b) shows the sinusoid electrical signal applied on the PZT cylinder generated by

the function generator.

For non-stationary vibration measurement, a sinusoid signal with frequency from 500Hz to 1 kHz and one sweep time 0.05s generated by the function generator is continuously applied on the PZT cylinder. Figure 6.5 is the position information of the sweep non-stationary vibration signal determined by the global wavelet power spectrum using the digital low pass filter with different cutoff frequency. As similar as the stationary vibration case, the SNR of the 200MHz and 350MHz filters are 19.8dB and 15.9dB respectively which means 4dB SNR improvement by using the 200MHz filter. We can also find the frequency range of the vibration event at the vibration position but the time-dependent information has already been missed in the global wavelet power spectrum.

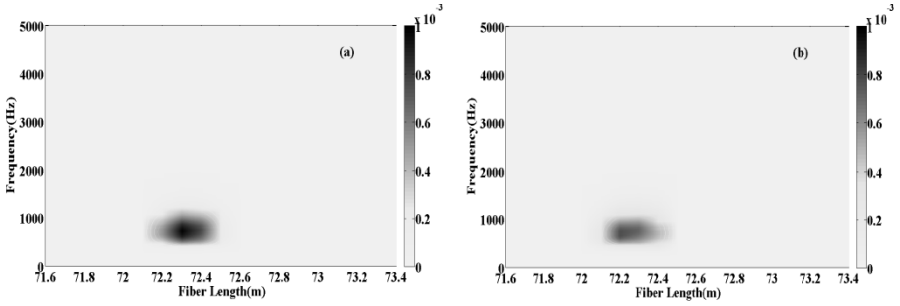

Figure 6.5: Contour plot of the global wavelet power spectrum along the fiber length for the non-stationary vibration detection of 500Hz-1000Hz sweep signal (a) 200MHz low pass filter (b) 350MHz low pass filter.

Figure 6.6 presents the frequency evolution with time increasing from 500Hz to 1000Hz linearly in a time section 0.05s. Figure 6.6(a) is the scalogram of the sweep signal corresponding to two sweep periods. Similar to the stationary case, the instantaneous

frequency of the sweep signal is shown in Figure 6.6(b) and the inset graph in Figure 6.6(b) shows the sweep electrical signal driving the PZT cylinder.

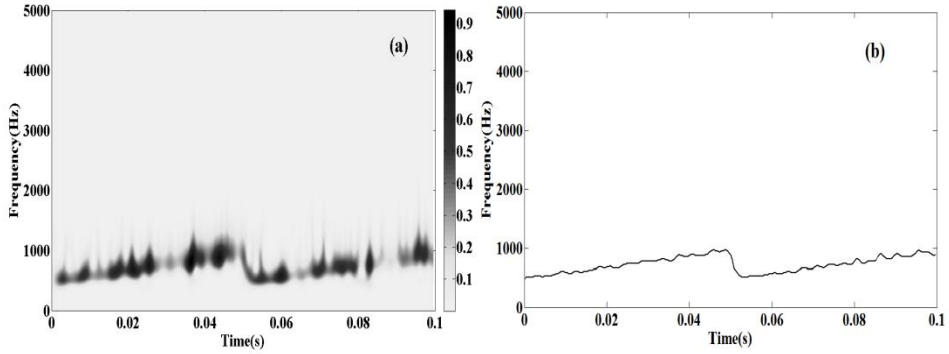

Figure 6.6: (a) Scalogram of the 500Hz-1000Hz sweep non-stationary vibration event at the vibration position (b) instantaneous frequency obtained by wavelet ridge detection.

6.5 Conclusions

The application of continuous wavelet transform to analyze the non-stationary signal in the distributed vibration sensing based on phase-sensitive OTDR system is demonstrated in this chapter. The frequency evolution with time of a sweep sinusoid vibration signal is found from the scalogram through the CWT method. This reported time-frequency analysis scheme is proved to be a powerful tool to evaluate both the stationary and non-stationary vibration events using the phase OTDR system for damage detection of civil or mechanical structures.

Chapter 7

7 Distributed vibration sensing with time-resolved optical frequency-domain reflectometry

This chapter presents a new method proposed by our group for distributed measurement of vibration event with high spatial resolution based on optical frequency-domain reflectometry [88]. I worked together with Dr. Da-peng Zhou to build the experimental setup and vibration test platform and perform the experiment. We conducted the data analysis together. Section 7.1 introduces the research background related to this new technique. Fundamental principle of OFDR is present in Section 7.2. The signal processing method and the experimental setup are shown in Section 7.3. Section 7.4 presents the experimental results of position and frequency information for a PZT vibration event.

7.1 Introduction

In prior chapters we discussed the distributed vibration system based on phase-sensitive OTDR technique. The spatial resolution of the OTDR measurement is mainly determined by the probe pulse width. A narrow pulse is preferred for a high spatial resolution. According to Eq. (2.18), the Rayleigh backscattering light dependents on the energy of the pulse $P_0 \cdot T$. The Rayleigh backscattering signal will become smaller if the pulse width

decreases under the same pules peak power. Therefore, the commonly-used pulse is on the order of 10ns limited by the SNR of the system. Spatial resolution of phase-sensitive OTDR is limited on the order of meters, which might not be adequate for some applications in aerospace which require centimeter spatial resolution. In this chapter, distributed vibration information is accessed using time-resolved OFDR. Time-domain information is obtained by measuring Rayleigh backscattering spectrum in different wavelength spans which falls in successive time sequence due to the linear frequency sweep of the tunable laser source with a constant tuning rate. The local Rayleigh backscattering spectrum shift in time sequence could be used to determine dynamic strain information at a specific position of the vibrated state with respect to that of the non-vibrated state along the fiber length. Standard single-mode fiber is used as sensing head, while the measurable frequency range of 0-32 Hz with the spatial resolution of 10 cm is demonstrated up to total length of 17 m.

7.2 Fundamental principle of OFDR

OFDR technique is one of the most powerful tools for fiber device characterization and optical fiber sensing. Compared to the OTDR technique, OFDR can achieve high sensitivity and high spatial resolution on the order of hundreds of micrometers[28]. The essential part of the OFDR system is a wavelength-swept homodyne interferometry. Optical frequency of a tunable laser source (TLS) is scanned linearly and the light is sent through the two arms of the interferometer by an optical coupler. The beat signal

generated by the optical interference between a measurement sensing arm and a reference arm which is also called local oscillator (LO) is collected by an optical detector. The signals from the measurement arm consist of different reflected lights coming from the fiber component under test. The beat frequency is proportional to the distance between the LO light and the reflection light along the sensing fiber. Therefore the response in the spectral domain of the fiber under test will be obtained and processed into the time domain by the FFT.

One problem which can affect the spatial resolution and the maximum detectable range of OFDR system is the nonlinearity of the sweeping rate of the TLS. In practice, the available laser source always has some turning fluctuations and cannot implement a strict linear sweeping with time. This deterioration of the detection performance due to the nonlinear turning characteristic can be mitigated by a well-known trigger interferometer technique [28]. By using an auxiliary Mach-Zehnder interferometer which can determine the variation of the instantaneous optical frequency, the data could be sampled in the equal frequency-domain intervals rather than the time-domain intervals. Commonly, the zero-crossing point of the interference signals from the trigger interferometer is used as a sampling clock for the data acquisition of the measurement interferometer by setting a suitable threshold value.

The sensitivity of the reflectometry measuring technique based on the coherent detection scheme is greatly improved compared to the conventional time domain method. However a fundamental problem called polarization-induced signal fading will exist due to the

mismatch of the state of polarization between the two arms of the interferometer. Considering one extreme situation, the signal will completely disappear if the SOP of the light coming from the reference arm and a given reflection along the sensing arm are orthogonal with each other. Hence, one effective method to avoid this polarization mismatch induced signal fading is the polarization diversity schemeby splitting the electric field of the reference arm into two orthogonal SOP. The addition of the two polarization elements detected by two optical detectors can result in a summed signal without the polarization dependence.

The maximum detectable length of the fiber under test (FUT), $L_{\max}$ is determined by the differential time delay of the trigger interferometer using the Nyquist sampling criteria by [28]

$$L_{\max} = \frac{c\tau_g}{4n_g}, \tag{7.1}$$

where c is the velocity of light in vacuum; n_g is the group index of FUT; τ_g is the group delay introduced by the trigger interferometer and the factor 4 is due to the sampling theorem and the double-pass nature of the measurement interferometer.

The spatial resolution ΔL is determined by the wavelength scan range $\Delta\lambda_{\mathrm{TLS}}$ of the TLS swept in the measurement which is shown in Eq. (7.2) as following

$$\Delta L \approx \frac{\lambda^2}{2n_g \Delta\lambda_{\mathrm{TLS}}}, \tag{7.2}$$

where λ is the central operating wavelength of the TLS. We can find a higher spatial resolution could be obtained by a wider wavelength scan range.

7.3 Experiment setup and signal processing method

The experimental configuration used for vibration measurement is schematically shown in Figure 7.1. The OFDR system consists of a TLS working under the continuous sweep mode with a 100 kHz linewidth around 1550nm range. An auxiliary Mach-Zehnder interferometer is adopted to remove laser tuning errors from the data. When the wavelength of the TLS is scanning, the beat signal from the combination of the Rayleigh scattering signal and the local oscillator light is split by a polarization beam splitter (PBS). The two orthogonal components “s” and “p” are collected by two photo detectors and sampled with equal frequency intervals. Fourier transform is then used to convert these frequency data into time-domain data which could be scaled to the length of FUT; after performing a vector sum of the transformed “s” and “p” components, the Rayleigh backscatter pattern versus the length of the FUT could be obtained.

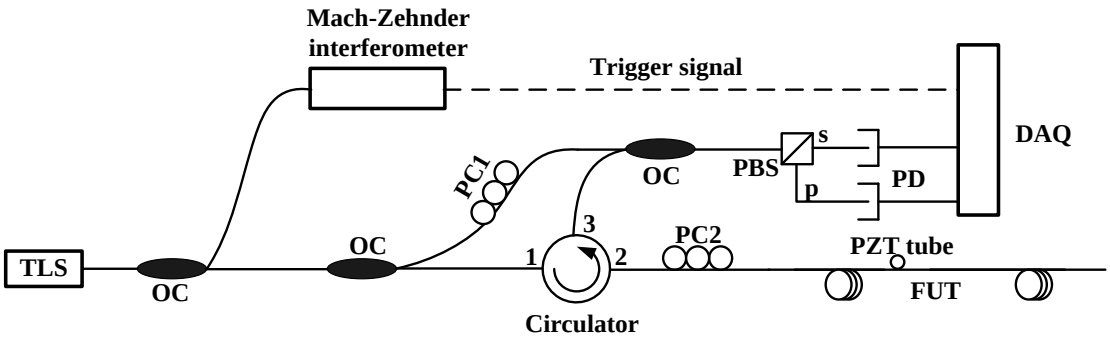

Figure 7.1: Experimental setup. TLS: tunable laser source; DAQ: data acquisition; OC: optical coupler; PC: polarization controller; PD: photodetector; PBS: polarization beam splitter; FUT: fiber under test; PZT: Lead zirconade titanate.

Figure 7.2 shows the flow chart of the vibration measurement procedure using time-resolved OFDR. Two groups of raw data are acquired by two times of system running; one is with the non-vibrated state and the other one is with the vibrated state. Each group of the data is divided evenly into N portions according to the time sequence which is corresponding to successive wavelength windows. Sampling rate for the vibration signal applied on the FUT is determined by the number of the data portions. Assuming total time for one sweep is T s, the sampling rate could be N/T Hz which would give the maximum measurable frequency of N/(2T) Hz according to Nyquist sampling theorem. FFT is performed on each portion of the two groups of data and the OTDR-like traces including the response of the Rayleigh backscattering for the scanned wavelength range along the sensing fiber is obtained. A small section of the time-domain data, which corresponds to a

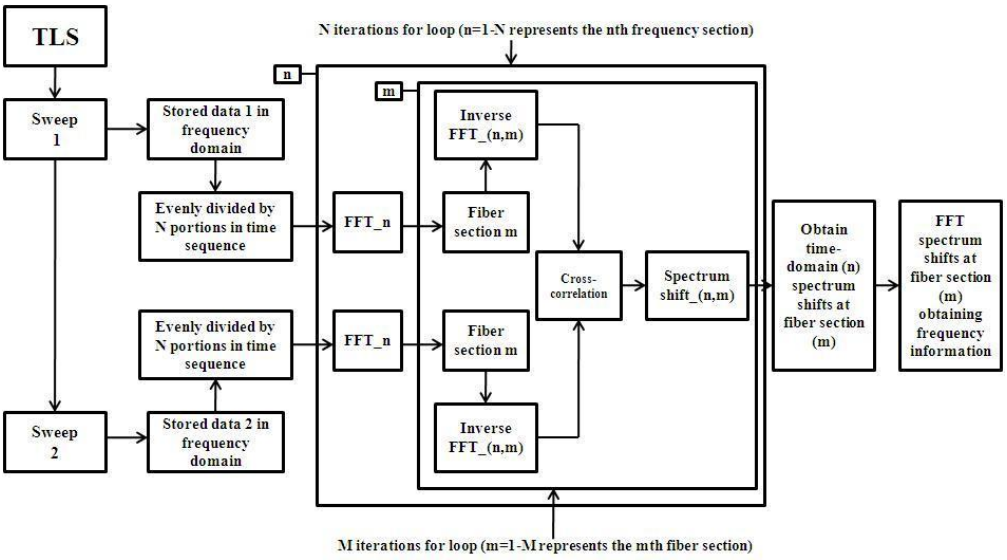

Figure 7.2: Flow chart of the distributed vibration measurement with optical frequency-domain reflectometry. TLS: tunable laser source; FFT: fast Fourier transforms

fiber region determined the spatial resolution of the vibration measurement, is chosen from the first time slot T/N of the data under the vibrated state. The local spectrum of the Rayleigh backscattering is retrieved through inverse Fourier transform. After performing cross-correlation calculation with the spectrum chosen from the same time slot data of the non-vibrated state, the spectrum shift of the Rayleigh backscatter indicating the strain change at that time slot could be obtained. This step is repeated by N times to obtain the variation information at the chosen fiber section for the total T s at a sampling rate of N/T Hz. Fourier transform of this time-domain signal will provide the frequency information of the vibration event. Next, all the other fiber sections' information could be obtained in the similar way realizing the distributed dynamic strain measurement.

7.4 Experimental results and discussion

A trigger interferometer with a 70m path length difference is used in our experiment which means that the maximum sensing length is around 17m determined by Eq. (7.2). The SMF sensing fiber is 10.8m long and a small circle is made at the end of it to reduce the Fresnel reflection. The vibration source is a PZT cylinder with a diameter of 30mm and the fiber section wrapped on the surface is about 20cm. The CW light power launched into the sensing fiber is 2mW. The wavelength scanning rate and the scanning range of the TLS are 40nm/s and 50nm respectively which give us that scan time for one sweep is T=1.25 s and a spatial resolution of 0.016 mm between the two adjacent data points. Figure 7.3 shows the Rayleigh backscatter signals as a function of fiber length after vector sum of the “s” and “p” components with different wavelength windows.

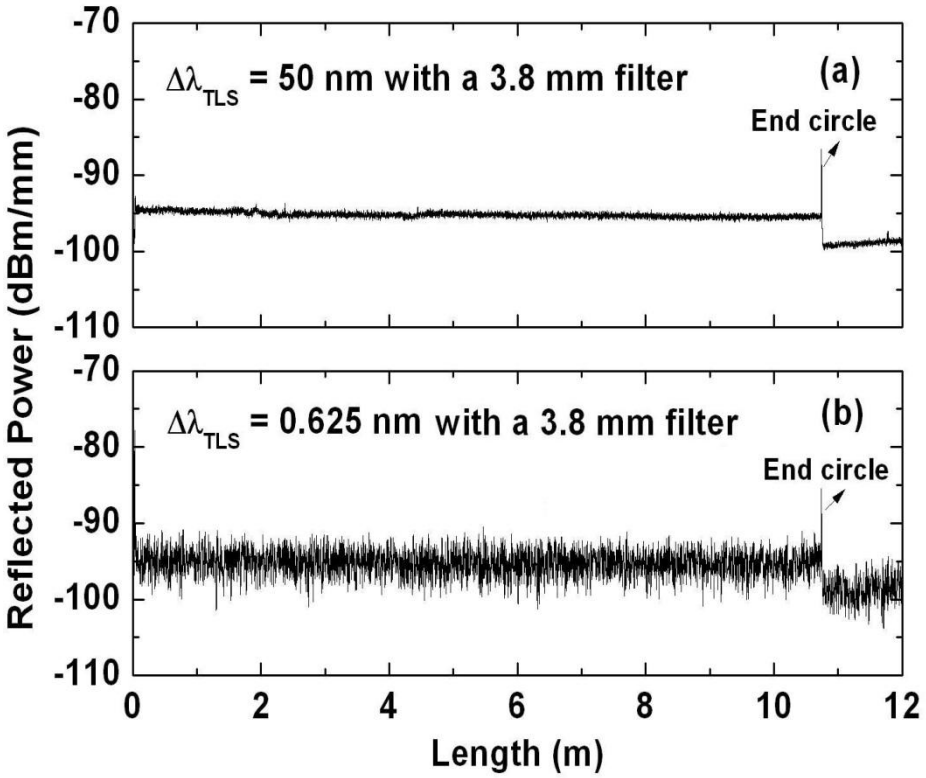

Figure 7.3: Rayleigh backscatter as a function of fiber length with the TLS sweeping range of (a) 50 nm and (b) 0.625 nm. Both the curves are vector sum of the "s" and "p" components and a 3.8 mm filter is used for both cases.

In Figure 7.3(a) all the data points corresponding to total 50nm wavelength window are processed by FFT to be converted into the time-domain and then scaled along the fiber length. We can find the OTDR-like trace shows a smooth profile after a 3.8mm moving average filter is applied. After that, the frequency-domain data is evenly divided by N=80 portions in time sequence, only the first part (first time slot) of the data corresponding to a wavelength window 0.625nm is used to perform Fourier transform and then scaled to fiber length. The OTDR curve is shown in Figure 7.3 (b) with a spatial resolution of 1.28 mm between two adjacent data points. Although the same moving average filter is applied, the curve in Figure 7.3 (b) still has a relatively large fluctuation due to the limited points within the 3.8mm length.

In the following, the Rayleigh backscatter spectrum shift obtained by the cross-correlation of the data between the reference scan and the measurement scan at the vibration position of the fiber (4.26 m) within several different time slots is shown in Figure 7.4 when a 5 Hz sinusoidal voltage is applied on the PZT tube. The position of the cross-correlation peak represents the spectrum shift of the Rayleigh backscattering light. Two different fiber lengths corresponding to two different spatial resolutions are studied for comparison. The better the spatial resolution is, the worse the signal-to-noise ratio becomes as indicated in Figure 7.4. In the meantime, the spectral accuracy of the Rayleigh backscattering spectrum is inversely proportional to the spatial resolution. From Figure 7.4, the peak movement at different time is observed which is caused by the external vibration. After locating the peak position of the spectrum shift obtained by quadratic least square fitting at all the time slots at a particular fiber position, time-domain spectrum shift or time varied applied strain (~1 με/pm) could be obtained as shown in Figure 7.5. Two different positions are indicated when a 5 Hz vibration is applied on the PZT tube. At the vibrated position of 4.26 m, a sinusoidal varied spectrum shift could be clearly seen in Figure 7.5(a) and (b) for both the 20 cm and 10 cm spatial resolution. At the non-vibrated position of 4.48 m, no significant variation could be observed as shown in Figure 7.5(c) and (d).

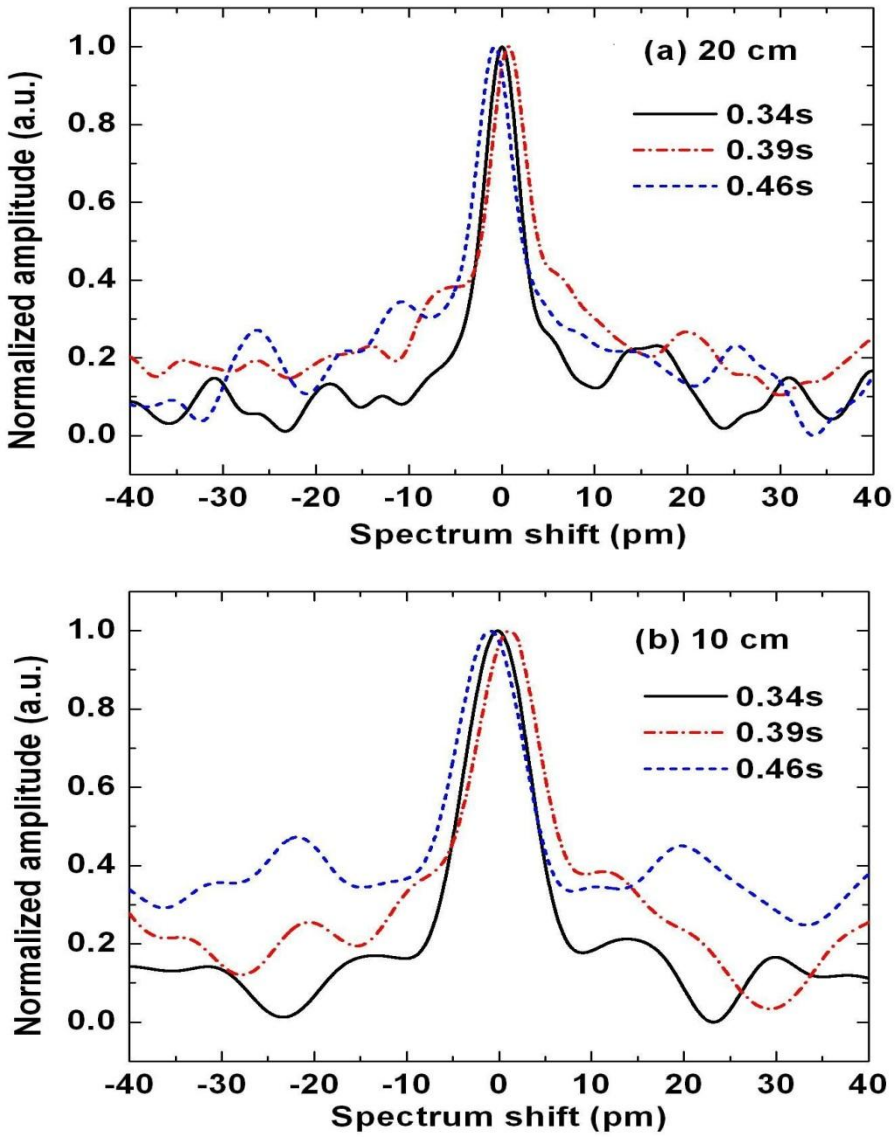

Figure 7.4: Rayleigh backscatter spectrum shift obtained by cross-correlation within different time slots with (a) 20 cm and (b) 10 cm spatial resolution at the vibrated position of 4.26 m when a 5 Hz sinusoidal voltage is applied to the PZT tube.

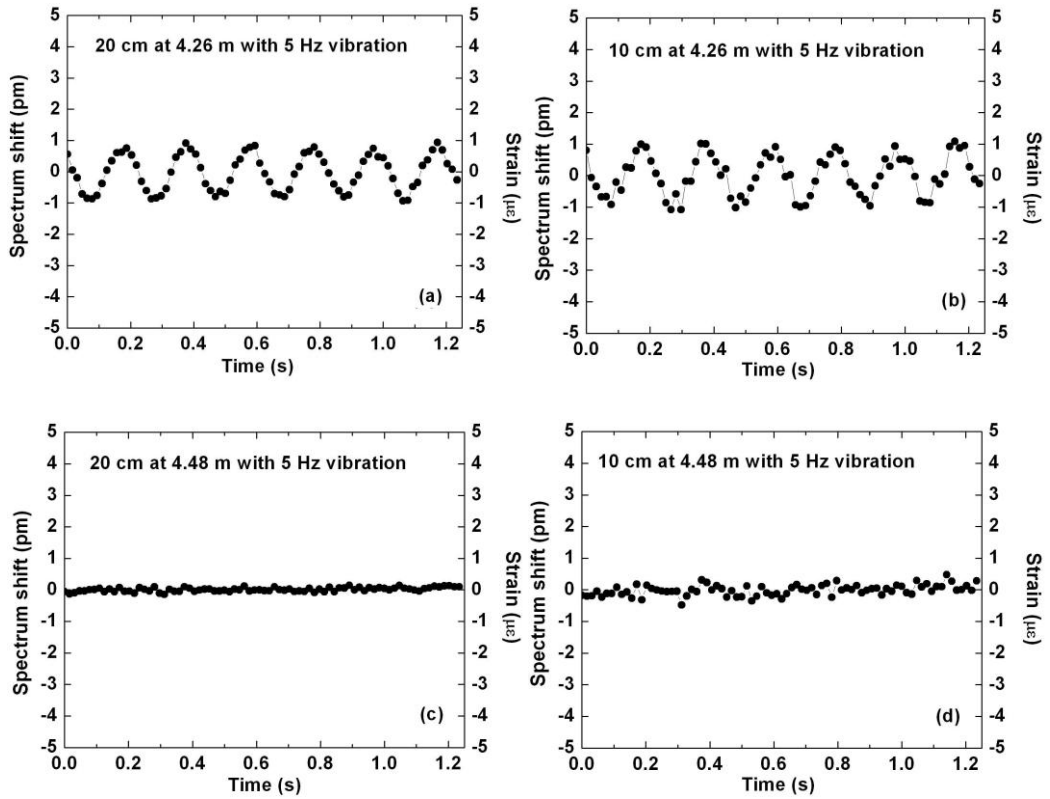

Figure 7.5: Time-domain Rayleigh backscatter spectrum shift (applied strain) at vibrated position 4.26 m of (a) 20 cm (b) 10 cm spatial resolution; non-vibrated position at 4.48 m of (c) 20 cm (d) 10 cm spatial resolution when a 5 Hz sinusoidal voltage is applied to the PZT tube.

Note that, for 10 cm resolution, relatively larger noise in the time-domain signal attributes to low signal-to-noise ratio. Repeated experiment confirms that 10 cm resolution is readily achievable for vibration measurement. Even a 8 cm resolution could also be achieved but with a poor single-to-noise ratio. In the following illustration, we choose 10 cm resolution for the measurement. Figure 7.6 shows the time-domain Rayleigh backscatter spectrum shift at vibrated position of 4.26 m with 10 cm resolution when a (a) 10 Hz and (b) 20 Hz sinusoidal voltage is applied to the PZT tube. The signal appeared in Figure 7.6(b) is not as

good as those of 5 Hz and 10 Hz, because the sampling rate is relatively slower; however, it is still enough to find the frequency information of such signal by fast Fourier transform. Finally, we investigate the distributed vibration measurement as shown in Figure 7.7 with different vibration frequencies applied to the PZT tube. The figures are contour plots of power spectrum (log unit) of the time-domain strain signal along the fiber length with a 10 cm spatial resolution. Clearly, both the frequency and position information could be resolved. The vibration length is 20 cm consistent with the fiber length wound on the PZT tube.

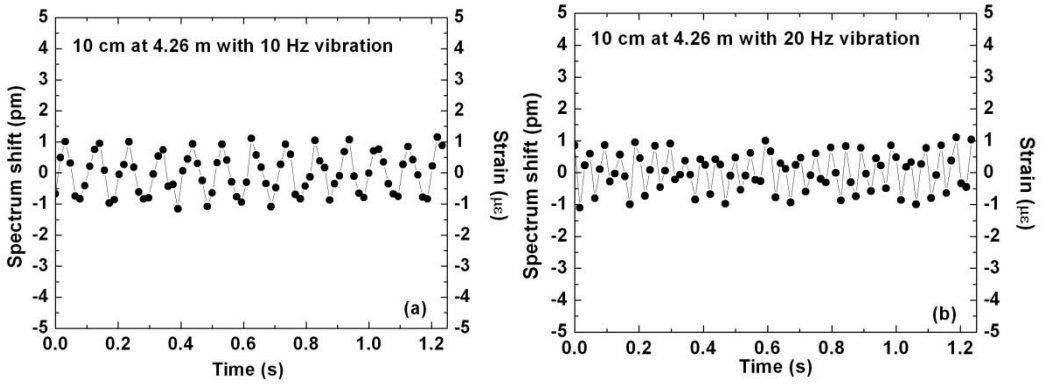

Figure 7.6: Time-domain Rayleigh backscatter spectrum shift (applied strain) at vibrated position 4.26 m with 10 cm spatial resolution when a (a) 10 Hz and (b) 20 Hz sinusoidal voltage is applied to the PZT tube.

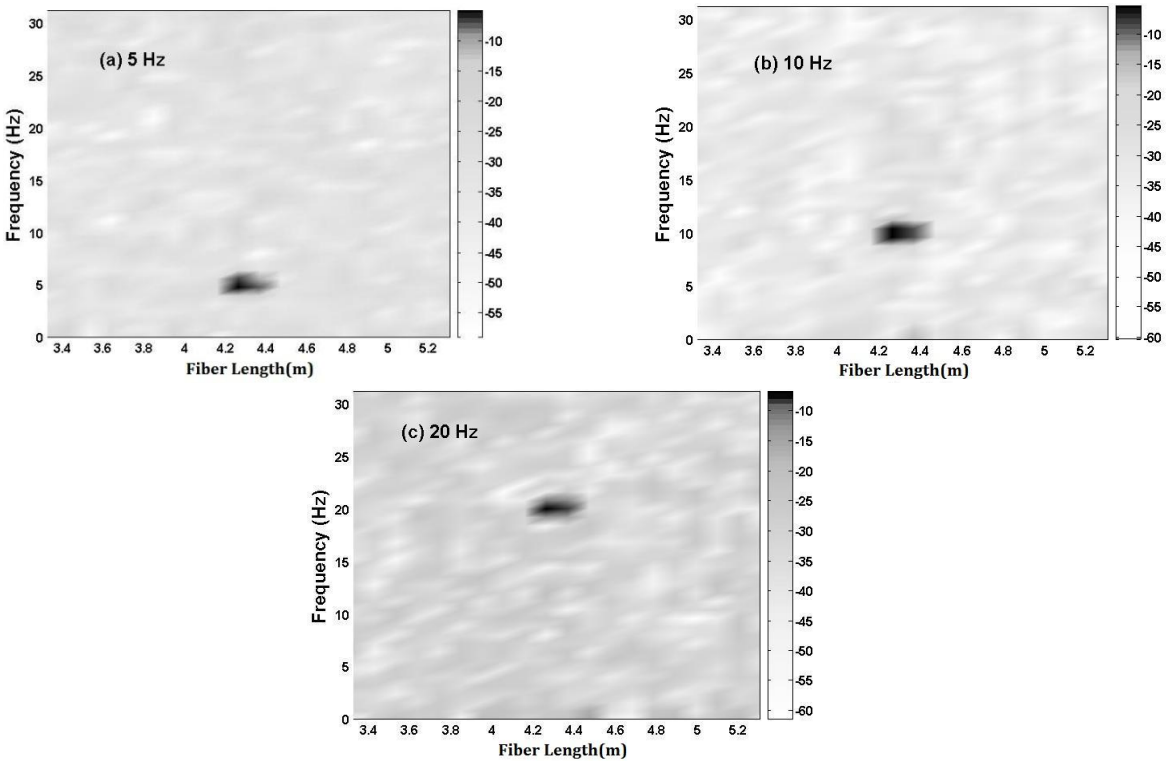

Figure 7.7: Contour plot of the power spectrum (log unit) of the time-domain strain signal along the fiber length for vibration frequency of (a) 5 Hz, (b) 10 Hz, and (c) 20 Hz, respectively.

7.5 Conclusions

A distributed optical fiber sensor which could measure vibration has been demonstrated. The measurement is achieved through time-resolved OFDR. By determining the spectrum shift of the Rayleigh backscatter distributed along the fiber length of the vibrated state with respect to that of the non-vibrated state, dynamic strain information could be obtained. 10 cm spatial resolution of 17 m sensing length is demonstrated. The measurable frequency range is 0-32 Hz. The frequency range, spatial resolution, and the sensing length could be improved provided with larger sweeping range, faster sweeping speed of the TLS with

proper delay length in the trigger interferometer. The reported approach makes the OFDR system a powerful tool for both the stationary and dynamic strain measurement with one simple setup and only two repeated measurements.

Chapter 8

8 Conclusion

8.1 Thesis outcomes

This thesis mainly focuses on developing and building distributed vibration fiber sensor with high spatial resolution and broad frequency response range based on Rayleigh backscattering light.

A phase-OTDR sensing system using all polarization-maintaining fiber components for higher frequency response, distributed vibration measurement has been firstly proposed. The polarization induced signal fading problem can be mitigated so that the position information can be determined with moving averaging time of 4. As a consequence the highest frequency response is improved to 2.25 kHz and the spatial resolution increases to 1m. Meanwhile, the former fiber loops setup for pencil-break detection is replaced by a new layout of a straight line sensing fiber which is more practical. The interacting length of fiber and disturbance is decreased to 0.13m. The maximum distance between vibration event and the sensing fiber is 18cm with a SNR larger than 2dB.

The ability of the moving average method to reduce the noise is proved to be one of the critical factors for further improving the performance of distributed vibration sensing. Therefore, wavelet denoising method is described to the distributed vibration sensing in

phase-sensitive OTDR system. Amplitude changes induced by the external vibration can be extracted from the excessive noise background effectively by wavelet denoising method compared to the moving averaging method. Thanks to the superior advantages of this new signal processing method, a vibration event up to 8 kHz using PZT cylinder is measured with a spatial resolution of 0.5m.

A new distributed fiber vibration sensor based on time-division multiplexing technique is proposed to increase the frequency response range of vibration detection. A designed probe waveform consisting of a short pulse and a quasi-CW lightwave is used to accomplish phase OTDR and polarization diversity scheme, respectively. The amplitude variation of Rayleigh backscattering traces induced by a very high frequency vibration event can be acquired even the pulse repetition rate is much shorter than the signal frequency. Measurement of a PZT vibration event with frequency up to 0.6MHz is successfully demonstrated.

We investigate the non-stationary vibration events using the phase-OTDR system based on continuous wavelet transform. Compared to the commonly-used FFT scheme which can only find the frequency distribution of the vibration and lose the time dependent information, frequency evolution with time can be obtained from the scalogram by CWT method. A new algorithm is proposed to determine the position information using the global wavelet power spectrum. A PZT vibration driven by a sweep sinusoid signal is analyzed to explore the information of frequency variation with time.

Besides the phase-sensitive OTDR system, we also investigate the feasibility of OFDR

system for distributed dynamic sensing. For the first time to the best of our knowledge, we propose a time-resolved OFDR with high spatial resolution to achieve distributed vibration sensing. Time-domain information is obtained by measuring Rayleigh backscatter spectrum in different wavelength span. The local Rayleigh backscatter spectrum shift in time sequence could be used to determine dynamic strain information at a specific position of the vibrated state with respect to that of the non- vibration state. Vibration events with frequency range 0-32Hz can be successfully measured with 10cm spatial resolution along a 17m single-mode sensing fiber.

The performance of the distributed vibration sensor based on Rayleigh backscattering is summarized in Table 8.1. Compared to the other available distributed vibration fiber sensors, phase-sensitive OTDR can achieve distributed vibration sensing with high frequency response and high spatial resolution. Time-resolved OFDR can measure vibration event with a high spatial resolution of 0.1m.

	Fiber Type	Spatial Resolution	Sensing Length	Frequency Range	Non-stationary Detection
Phase OTDR based on all PM configuration[80]	PMF	1m	200m	Up to 2.25kHz	No
Phase OTDR using wavelet denoising[86]	SMF	0.5m	1km	Up to 8kHz	No
TDM phase OTDR	SMF	1m	680m	Up to 600kHz	No
Phase OTDR using CWT[85]	SMF	0.2m	200m	500-1000Hz	Yes
Time-resolved OFDR[88]	SMF	0.1m	17m	0-30Hz	No

Table 8.1:Performance of distributed vibration fiber sensor based on Rayleigh backscattering.

8.2 Future work

Some possible future research directions are presented as follows.

In Chapter 3, we demonstrated the capability of measuring multiple disturbances simultaneously for our phase-sensitive OTDR by using two pencil-break events. This is one of the most attractive advantages for a truly distributed sensor. However, two vibration events is usually not good enough in real applications such as the health monitoring of the large hydro power generators used in electric utility plants which several hundreds of windings need to be monitored at a reasonable cost. We need to test the performance of the

phase OTDR under several of vibration events that occur at the same time to see whether cross talk and signal deterioration exist.

For the phase-sensitive OTDR system for vibration detection, coherent detection scheme is utilized in order to improve the SNR because the backscattered Rayleigh signals of the narrow pulses are very weak. However, the polarization state mismatching between the signal arm and local oscillator arm will lead to the deterioration of Rayleigh backscattering signal especially when the SOP of the fiber region under the vibration is almost orthogonal with the local oscillator arm. One possible method is to use direct detection scheme instead of coherent detection which is polarization independent.

For our distributed vibration sensor based on time-resolved OFDR presented in Chapter 7, a reference scan is need when there is no any disturbance along the fiber under test to perform the cross-correlation with the scan under vibration in order to find the spectrum shift induced by the vibration. However, this step is difficult to accomplish in real applications for dynamic measurements since the interested events change very fast. One possible solution for this problem is to replace the single mode fiber with polarization maintaining fiber. Autocorrelation can be performed to find the side peak shift which represented the coupling between the two orthogonal polarization modes in PMF which means the reference scan is not necessary.

Bibliography

1. C. R. Farrar, S. W. Doebling, and D. A. Nix, "Vibration-based structural damage identification," ***Philosophical Transactions of the Royal Society of London Series a-Mathematical Physical and Engineering Sciences*** **359**, 131-149 (2001).

2. Y. Zou, L. Tong, and G. P. Steven, "Vibration-based model-dependent damage (delamination) identification and health monitoring for composite structures - A review," ***Journal of Sound and Vibration*** **230**, 357-378 (2000).

3. Y. J. Yan, L. Cheng, Z. Y. Wu, and L. H. Yam, "Development in vibration-based structural damage detection technique," ***Mechanical Systems and Signal Processing*** **21**, 2198-2211 (2007).

4. X. Y. Bao, C. S. Zhang, W. H. Li, M. Eisa, S. El-Gamal, and B. Benmokrane, "Monitoring the distributed impact wave on a concrete slab due to the traffic based on polarization dependence on stimulated Brillouin scattering," ***Smart Materials & Structures*** **17**(2008).

5. R. Bernini, A. Minardo, G. Testa, and L. Zeni, "Dynamic strain measurements on a cantilever beam using stimulated Brillouin scattering," ***Smart Materials & Structures*** **19**(2010).

6. K. O. Hill and G. Meltz, "Fiber Bragg grating technology fundamentals and overview," ***Journal of Lightwave Technology*** **15**, 1263-1276 (1997).

7. A. D. Kersey, M. A. Davis, H. J. Patrick, M. LeBlanc, K. P. Koo, C. G. Askins, M. A. Putnam, and E. J. Friebele, "Fiber grating sensors," ***Journal of Lightwave Technology*** **15**, 1442-1463 (1997).

8. N. Takahashi, K. Yoshimura, and S. Takahashi, "Detection of ultrasonic mechanical vibration of a solid using fiber Bragg grating," ***Japanese Journal of Applied Physics Part 1-Regular Papers Short Notes & Review Papers*** **39**, 3134-3138 (2000).

9. A. D. Kersey, T. A. Berkoff, and W. W. Morey, "High-Resolution Fiber-Grating Based Strain Sensor with Interferometric Wavelength-Shift Detection," ***Electronics Letters*** **28**, 236-238 (1992).

10. T. Yoshino, K. Kurosawa, K. Itoh, and T. Ose, "Fiberoptic Fabry-Perot-Interferometer and Its Sensor Applications," ***IEEE Journal of Quantum Electronics*** **18**, 1624-1633 (1982).

11. A. D. Kersey, D. A. Jackson, and M. Corke, "A Simple Fiber Fabry-Perot Sensor," ***Optics Communications*** **45**, 71-74 (1983).

12. T. K. Gangopadhyay, P. J. Henderson, and A. D. Stokes, "Vibration monitoring by using a dynamic proximity sensor with interferometric encoding," ***Applied Optics*** **36**, 5557-5561 (1997).

13. T. K. Gangopadhyay and P. J. Henderson, "Vibration: history and measurement with an extrinsic Fabry-Perot sensor with solid-state laser interferometry," ***Applied Optics*** **38**, 2471-2477 (1999).

14. L. A. Gao, S. C. Liu, Z. W. Yin, L. A. Zhang, L. Chen, and X. F. Chen, "Fiber-Optic Vibration Sensor Based on Beat Frequency and Frequency-Modulation Demodulation Techniques," ***IEEE Photonics Technology Letters*** **23**, 18-20 (2011).

15. H. V. Thakur, S. M. Nalawade, Y. Saxena, and K. T. V. Grattan, "All-fiber embedded PM-PCF vibration sensor for Structural Health Monitoring of composite," ***Sensors and Actuators a-Physical*** **167**, 204-212 (2011).

16. S. J. Spammer, P. L. Swart, and A. A. Chtcherbakov, "Merged Sagnac-Michelson interferometer for distributed disturbance detection," ***Journal of Lightwave Technology*** **15**, 972-976 (1997).

17. S. J. Russell, K. R. C. Brady, and J. P. Dakin, "Real-time location of multiple time-varying strain disturbances, acting over a 40-km fiber section, using a novel dual-Sagnac interferometer," ***Journal of Lightwave Technology*** **19**, 205-213 (2001).

18. X. J. Fang, "Fiber-optic distributed sensing by a two-loop Sagnac interferometer," ***Optics Letters*** **21**, 444-446 (1996).

19. M. Farhadiroushan., T. R. Parker., and S. Shatalin., "Method and apparatus for optical sensing," (2012).

20. X. Y. Bao and L. Chen, "Recent Progress in Distributed Fiber Optic Sensors," ***Sensors*** **12**, 8601-8639 (2012).

21. R. Bernini, A. Minardo, and L. Zeni, "Dynamic strain measurement in optical fibers by stimulated Brillouin scattering," ***Optics Letters*** **34**, 2613-2615 (2009).

22. M. Hobel, J. Ricka, M. Wuthrich, and T. Binkert, "High-Resolution Distributed Temperature Sensing with the Multiphoton-Timing Technique," ***Applied Optics*** **34**, 2955-2967 (1995).

23. K. Shimizu, T. Horiguchi, Y. Koyamada, and T. Kurashima, "Coherent Self-Heterodyne Detection of Spontaneously Brillouin-Scattered Light Waves in a Single-Mode Fiber," ***Optics Letters*** **18**, 185-187 (1993).

24. Y. K. Dong, H. Y. Zhang, L. Chen, and X. Y. Bao, "2 cm spatial-resolution and 2 km range Brillouin optical fiber sensor using a transient differential pulse pair," ***Applied Optics*** **51**, 1229-1235 (2012).

25. Y. K. Dong, L. Chen, and X. Y. Bao, "Extending the Sensing Range of Brillouin Optical Time-Domain Analysis Combining Frequency-Division Multiplexing and In-Line EDFAs," ***Journal of Lightwave Technology*** **30**, 1161-1167 (2012).

26. K. Y. Song, W. W. Zou, Z. Y. He, and K. Hotate, "All-optical dynamic grating generation based on Brillouin scattering in polarization-maintaining fiber," ***Optics Letters*** **33**, 926-928 (2008).

27. M. Froggatt and J. Moore, "High-spatial-resolution distributed strain measurement in optical fiber with Rayleigh scatter," ***Applied Optics*** **37**, 1735-1740 (1998).

28. B. J. Soller, D. K. Gifford, M. S. Wolfe, and M. E. Froggatt, "High resolution optical frequency domain reflectometry for characterization of components and assemblies," ***Optics Express*** **13**, 666-674 (2005).

29. Y. Peled, A. Motil, and M. Tur, "Fast Brillouin optical time domain analysis for dynamic sensing," ***Optics Express*** **20**, 8584-8591 (2012).

30. Z. Y. Zhang and X. Y. Bao, "Distributed optical fiber vibration sensor based on spectrum analysis of Polarization-OTDR system," ***Optics Express*** **16**, 10240-10247 (2008).

31. R. W. Boyd, *Nonlinear optics*, 3rd ed. (Academic Press, Amsterdam ; Boston, 2008).

32. G. P. Agrawal, *Fiber-optic communication systems*, 3rd ed., Wiley series in microwave and optical engineering (Wiley-Interscience, New York, 2002).

33. J. D. Jackson, *Classical electrodynamics*, 3rd ed. (Wiley, New York, 1999).

34. E. G. Neumann, "Analysis of the Backscattering Method for Testing Optical Fiber Cables," ***Aeu-Archiv Fur Elektronik Und Ubertragungstechnik-International Journal of Electronics and Communications*** **34**, 157-160 (1980).

35. D. Derickson, *Fiber optic test and measurement* (Prentice Hall PTR, Upper Saddle River, N.J., 1998).

36. J. Jasene, "The theory and application of fiber optic sensors with spread parameters" http://www.eaeeie.org/theiere_bratislava.

37. M. K. Barnoski and S. M. Jensen, "Fiber Waveguides - Novel Technique for Investigating Attenuation Characteristics," ***Applied Optics*** **15**, 2112-2115 (1976).

38. A. Hartog, "A distributed temperature sensor based on liquid-core optical fibers," ***Lightwave Technology, Journal of*** **1**, 498-509 (1983).

39. M. C. Farries, M. E. Fermann, R. I. Laming, S. B. Poole, and D. N. Payne, "Distributed Temperature Sensor Using Nd-3+-Doped Optical Fiber," ***Electronics Letters*** **22**, 418-419 (1986).

40. P. Healey and D. J. Malyon, "OTDR in Single-Mode Fiber at 1.5-Mu-M Using Heterodyne-Detection," ***Electronics Letters*** **18**, 862-863 (1982).

41. Y. Koyamada and H. Nakamoto, "High-Performance Single-Mode Otdr Using Coherent Detection and Fiber Amplifiers," ***Electronics Letters*** **26**, 573-575 (1990).

42. P. Healey, "Fading in Heterodyne Otdr," ***Electronics Letters*** **20**, 30-32 (1984).

43. H. Izumita, S. Furukawa, Y. Koyamada, and I. Sankawa, "Fading Noise-Reduction in Coherent Otdr," ***IEEE Photonics Technology Letters*** **4**, 201-203 (1992).

44. H. Izumita, Y. Koyamada, S. Furukawa, and I. Sankawa, "Stochastic amplitude fluctuation in coherent OTDR and a new technique for its reduction by stimulating synchronous optical frequency hopping," ***Journal of Lightwave***

Technology **15**, 267-278 (1997).

45. H. F. Taylor and C. E. Lee, "Apparatus and method for fiber optic intrusion sensing," (1993).

46. J. C. Juarez, E. W. Maier, K. N. Choi, and H. F. Taylor, "Distributed fiber-optic intrusion sensor system," ***Journal of Lightwave Technology*** **23**, 2081-2087 (2005).

47. W. Seo, "Fiber optic intrusion sensor investigation," (Texas A&M Univ, 1994).

48. A. J. Rogers, "Polarization Optical-Time Domain Reflectometry," ***Electronics Letters*** **16**, 489-490 (1980).

49. A. J. Rogers, "Polarization-Optical Time Domain Reflectometry - a Technique for the Measurement of Field Distributions," ***Applied Optics*** **20**, 1060-1074 (1981).

50. B. Y. Kim and S. S. Choi, "Backscattering Measurement of Bending-Induced Birefringence in Single-Mode Fibers," ***Electronics Letters*** **17**, 193-194 (1981).

51. R. E. Schuh, E. S. R. Sikora, N. G. Walker, A. S. Siddiqui, L. M. Gleeson, and D. H. O. Bebbington, "Theoretical-Analysis and Measurement of Effects of Fiber Twist on Polarization Mode Dispersion of Optical Fibers," ***Electronics Letters*** **31**, 1772-1773 (1995).

52. M. Wuilpart, P. Megret, M. Blondel, A. J. Rogers, and Y. Defosse, "Measurement of the spatial distribution of birefringence in optical fibers," ***IEEE Photonics Technology Letters*** **13**, 836-838 (2001).

53. J. Cameron, L. A. Chen, X. Y. Bao, and J. Stears, "Time evolution of polarization mode dispersion in optical fibers," ***IEEE Photonics Technology Letters*** **10**, 1265-1267 (1998).

54. D. S. Waddy, P. Lu, L. Chen, and X. Y. Bao, "Fast state of polarization changes in aerial fiber under different climatic conditions," ***IEEE Photonics Technology Letters*** **13**, 1035-1037 (2001).

55. F. Corsi, A. Galtarossa, and L. Palmieri, "Polarization mode dispersion characterization of single-mode optical fiber using backscattering technique,"

Journal of Lightwave Technology **16**, 1832-1843 (1998).

56. B. Huttner, B. Gisin, and N. Gisin, "Distributed PMD measurement with a polarization-OTDR in optical fibers," ***Journal of Lightwave Technology*** **17**, 1843-1848 (1999).

57. D. K. Gifford, M. E. Froggatt, M. S. Wolfe, S. T. Kreger, A. K. Sang, and B. J. Soller, "Millimeter resolution otpical reflectometry over up to two kilometers of fiber length," ***2007 Ieee Avionics, Fiber-Optics and Photonics Technology Conference***, 52-53 (2007).

58. A. J. Hymans and J. Lait, "Analysis of a frequency-modulated continuous-wave ranging system," ***Proceedings of the IEE - Part B: Electronic and Communication Engineering*** **107**, 365-372 (1960).

59. W. Eickhoff and R. Ulrich, "Optical Frequency-Domain Reflectometry in Single-Mode Fiber," ***Applied Physics Letters*** **39**, 693-695 (1981).

60. J. P. vonderWeid, R. Passy, G. Mussi, and N. Gisin, "On the characterization of optical fiber network components with optical frequency domain reflectometry," ***Journal of Lightwave Technology*** **15**, 1131-1141 (1997).

61. S. Kieckbusch, C. Knothe, and E. Brinkmeyer, "Fast and accurate characterization of fiber Bragg gratings with high spatial and spectral resolution," in *Optical Fiber Communications Conference, 2003. OFC 2003*, 2003), 379-381 vol.371.

62. G. D. Van Wiggeren, A. R. Motamedi, B. Szafraniec, R. S. Tucker, and D. M. Baney, "Single-scan polarization-resolved heterodyne optical network analyzer," in *Optical Fiber Communication Conference and Exhibit, 2002. OFC 2002*, 2002), 253-254.

63. M. Froggatt, "Distributed measurement of the complex modulation of a photoinduced Bragg grating in an optical fiber," ***Applied Optics*** **35**, 5162-5164 (1996).

64. S. T. Kreger, D. K. Gifford, M. E. Froggatt, B. J. Soller, and M. S. Wolfe, "High resolution distributed strain or temperature measurements in single- and multi-mode fiber using swept-wavelength interferometry," in *Optical Fiber Sensors*, (2006), p. ThE42.

65. S. H. Yun, G. J. Tearney, J. F. de Boer, N. Iftimia, and B. E. Bouma, "High-speed optical frequency-domain imaging," ***Optics Express*** **11**, 2953-2963 (2003).

66. X. Z. Wang, W. H. Li, L. Chen, and X. Y. Bao, "Distributed Mode Coupling Measurement Along Tapered Single-Mode Fibers With Optical Frequency-Domain Reflectometry," ***Journal of Lightwave Technology*** **30**, 1499-1508 (2012).

67. Y. L. Lu, T. Zhu, L. A. Chen, and X. Y. Bao, "Distributed Vibration Sensor Based on Coherent Detection of Phase-OTDR," ***Journal of Lightwave Technology*** **28**, 3243-3249 (2010).

68. M. E. Froggatt, D. K. Gifford, S. T. Kreger, M. S. Wolfe, and B. J. Soller, "Distributed Strain and Temperature Discrimination in Unaltered Polarization Maintaining Fiber," in *Optical Fiber Sensors,* (2006), p. ThE42.

69. W. W. Zou, Z. Y. He, and K. Z. Hotate, "Complete discrimination of strain and temperature using Brillouin frequency shift and birefringence in a polarization-maintaining fiber," ***Optics Express*** **17**, 1248-1255 (2009).

70. Y. K. Dong, L. Chen, and X. Y. Bao, "Truly distributed birefringence measurement of polarization-maintaining fibers based on transient Brillouin grating," ***Optics Letters*** **35**, 193-195 (2010).

71. N. J. Frigo, A. Dandridge, and A. B. Tveten, "Technique for Elimination of Polarization Fading in Fiber Interferometers," ***Electronics Letters*** **20**, 319-320 (1984).

72. K. H. Wanser and N. H. Safar, "Remote Polarization Control for Fiberoptic Interferometers," ***Optics Letters*** **12**, 217-219 (1987).

73. Z. K. Peng and F. L. Chu, "Application of the wavelet transform in machine condition monitoring and fault diagnostics: a review with bibliography," ***Mechanical Systems and Signal Processing*** **18**, 199-221 (2004).

74. S. G. Chang, B. Yu, and M. Vetterli, "Spatially adaptive wavelet thresholding with context modeling for image denoising," ***IEEE Transactions on Image Processing*** **9**, 1522-1531 (2000).

75. S. Santoso, E. J. Powers, and W. M. Grady, "Power quality disturbance data compression using wavelet transform methods," ***IEEE Transactions on Power***

***Delivery* 12**, 1250-1257 (1997).

76. S. G. Chang, B. Yu, and M. Vetterli, "Adaptive wavelet thresholding for image denoising and compression," ***IEEE Transactions on Image Processing* 9**, 1532-1546 (2000).

77. O. Rioul and M. Vetterli, "Wavelets and signal processing," ***IEEE Signal Processing Magazine* 8**, 14-38 (1991).

78. Y. Y. Tang, *Wavelet Theory and Its Application to Pattern Recognition* (World Scientific, 1999).

79. S. G. Mallat, *A wavelet tour of signal processing*, 2nd ed. (Academic Press, San Diego, 1999).

80. Z. G. Qin, T. Zhu, L. Chen, and X. Y. Bao, "High Sensitivity Distributed Vibration Sensor Based on Polarization-Maintaining Configurations of Phase-OTDR," ***IEEE Photonics Technology Letters* 23**, 1091-1093 (2011).

81. H. Y. Zhang, Y. K. Dong, J. Leeson, L. A. Chen, and X. Y. Bao, "High sensitivity optical fiber current sensor based on polarization diversity and a Faraday rotation mirror cavity," ***Applied Optics* 50**, 924-929 (2011).

82. Q. Z. Sun, D. M. Liu, H. Wang, and H. R. Liu, "Distributed fiber-optic vibration sensor using a ring Mach-Zehnder interferometer," ***Optics Communications* 281**, 1538-1544 (2008).

83. P. S. Addison, J. Walker, and R. C. Guido, "Time-Frequency Analysis of Biosignals A Wavelet Transform Overview," ***IEEE Engineering in Medicine and Biology Magazine* 28**, 14-29 (2009).

84. F. Al-Badour, M. Sunar, and L. Cheded, "Vibration analysis of rotating machinery using time-frequency analysis and wavelet techniques," ***Mechanical Systems and Signal Processing* 25**, 2083-2101 (2011).

85. Z. G. Qin, L. Chen, and X. Y. Bao, "Continuous wavelet transform for non-stationary vibration detection with phase-OTDR," ***Optics Express* 20**, 20459-20465 (2012).

86. Z. G. Qin, L. Chen, and X. Y. Bao, "Wavelet Denoising Method for Improving Detection Performance of Distributed Vibration Sensor," ***IEEE***

***Photonics Technology Letters* 24**, 542-544 (2012).

87. W. H. Li, X. Y. Bao, Y. Li, and L. Chen, "Differential pulse-width pair BOTDA for high spatial resolution sensing," ***Optics Express* 16**, 21616-21625 (2008).

88. D. P. Zhou, Z. G. Qin, W. H. Li, L. Chen, and X. Y. Bao, "Distributed vibration sensing with time-resolved optical frequency-domain reflectometry," ***Optics Express* 20**, 13138-13145 (2012).

Curriculum Vitae

Full name Zengguang Qin

Education Ph.D. (Jan.2009-present)
Department of Physics
University of Ottawa, Ottawa, Canada
Supervisor: Prof. Xiaoyi Bao

Ph.D. Student (Sep.2006-Dec.2008)
School of Information Science and Engineering
Shandong University, Jinan, P.R. China
Supervisor: Prof. Xingyu Zhang

B.E. (Sep.2002-Jul.2006)
School of Information Science and Engineering
Shandong University, Jinan, P.R. China

List of Publications

Journal Paper

1. **Zengguang Qin**, Liang Chen, and Xiaoyi Bao, Continuous wavelet transform for non-stationary vibration detection with phase-OTDR, Optics Express, 20 (18), pp. 20459-20465 (2012)

2. **Zengguang Qin**, Liang Chen and XiaoyiBao, Wavelet denoising method for improving detection performance of distributed vibration sensor, IEEE Photonics Technology Letter, 24 (7), pp.542-544 (2012)

3. **Zengguang Qin**, Tao Zhu, Liang Chen and XiaoyiBao, High Frequency Response Distributed Vibration Sensor Based on All Polarization-Maintaining Configurations of Phase-OTDR, IEEE Photonics Technology Letter, 23 (15), pp.1091-1093 (2011)

4. Da-Peng Zhou, **Zengguang Qin**, Wenhai Li, Liang Chen, and Xiaoyi Bao， Distributed vibration sensing with time-resolved optical frequency-domain reflectometry，Optics Express 20 (12), pp.13138-13145 (2012)

5. Yuangang Lu, **Zengguang Qin**, Ping Lu, Da-peng Zhou, Liang Chen ,Xiaoyi Bao， Distributed strain and temperature measurement by Brillouin beat spectrum in LEAF, IEEE Photonics Technology Letter, Submitted.

6. Yanping Xu, Ping Lu,**Zengguang Qin**, Jeremie Harris, Farhana Baset, Ping Lu, Vedula Ravi Bhardwaj, and Xiaoyi Bao, Vibration sensing using a tapered bend-insensitive fiber based Mach-Zehnder interferometer, Optics Express, Accept.

Conference paper and presentation:

1. **Zengguang Qin**, Liang Chen, and Xiaoyi Bao, Continuous wavelet transform for non-stationary vibration detection with phase-OTDR, 22nd International Conference on Optical Fiber Sensors, October 15-19 2012, Beijing (Poster)

2. Da-peng Zhou, **Zengguang Qin**, Liang Chen, and Xiaoyi Bao, High-spatial-resolution distributed vibration measurement using time-resolved optical frequency domain reflectometry, 22nd International Conference on Optical Fiber Sensors, October 15-19 2012, Beijing (Oral)

3. **Zengguang Qin**, Liang Chen, and Xiaoyi Bao, Distributed Vibration Sensor Based on Wavelet Signal Processing Method, Photonics North 2012, June 6-8 2012, Montreal (oral)

4. **Zengguang Qin**, Tao Zhu, Liang Chen, and Xiaoyi Bao, High Sensitivity Distributed Vibration Sensor Based on Polarization-Maintaining Configurations of Phase-OTDR, CIPI ANNUAL GENERAL MEETING, May 18-19 2011, Ottawa (oral)

5. Ryan Bolen, **Zengguang Qin**, Liang Chen, and Xiaoyi Bao, Optical Phase Diversity Detection to improve SNR in OFDR, CIPI ANNUAL GENERAL MEETING, June 3-4 2010, Niagara Falls (poster)